

TECHNICAL ADVANCES AND RESOURCES

A participant-derived xenograft model of HIV enables long-term evaluation of autologous immunotherapies

Chase D. McCann^{1,2*}, Christiaan H. van Dorp^{3*}, Ali Danesh^{1*}, Adam R. Ward^{4,5}, Thomas R. Dilling¹, Talia M. Mota¹, Elizabeth Zale², Eva M. Stevenson¹, Shabnum Patel^{6,7}, Chanson J. Brumme⁸, Winnie Dong⁸, Douglas S. Jones⁹, Thomas L. Andresen⁹, Bruce D. Walker^{10,11,12}, Zabrina L. Brumme^{8,13}, Catherine M. Bollard^{6,7}, Alan S. Perelson³, Darrell J. Irvine^{12,14,15,16}, and R. Brad Jones^{1,2}

HIV-specific CD8⁺ T cells partially control viral replication and delay disease progression, but they rarely provide lasting protection, largely due to immune escape. Here, we show that engrafting mice with memory CD4⁺ T cells from HIV⁺ donors uniquely allows for the in vivo evaluation of autologous T cell responses while avoiding graft-versus-host disease and the need for human fetal tissues that limit other models. Treating HIV-infected mice with clinically relevant HIV-specific T cell products resulted in substantial reductions in viremia. In vivo activity was significantly enhanced when T cells were engineered with surface-conjugated nanogels carrying an IL-15 superagonist, but it was ultimately limited by the pervasive selection of a diverse array of escape mutations, recapitulating patterns seen in humans. By applying mathematical modeling, we show that the kinetics of the CD8⁺ T cell response have a profound impact on the emergence and persistence of escape mutations. This “participant-derived xenograft” model of HIV provides a powerful tool for studying HIV-specific immunological responses and facilitating the development of effective cell-based therapies.

Introduction

Multiple lines of evidence have established a role for CD8⁺ HIV-specific T (HST) cells in partially controlling viral replication and delaying disease progression (Altfeld et al., 2006; Betts et al., 2006; Day et al., 2007; Turk et al., 2013; Turnbull et al., 2006). In a rare population termed “elite controllers” (~1% of individuals with HIV), CD8⁺ T cell responses contribute to exceptional control of viremia to below the limits of detection of conventional assays without antiretroviral (ARV) therapy (ART; Walker, 2007). Despite this potential, efforts to harness cellular immunity through vaccination or immunotherapy have yet to succeed in eliciting viremia control or in eliminating viral reservoirs that persist despite ART (Jones and Walker, 2016). In contrast, the treatments for many types of cancers are in the midst of a revolution, driven by the emergence of effective

immunotherapies including natural and engineered T cell therapies (June and Sadelain, 2018), immunomodulatory agents (Wei et al., 2018), and combinations thereof (Wang et al., 2019). A key contributor to these different trajectories has been the availability of informative small animal models of cancer, which have facilitated immunotherapeutic development in that field. By contrast, substantial barriers have limited the utility of animal models for studying cellular immunity to HIV.

Murine cells do not support HIV replication due to the absence of entry receptors, as well as multiple post-entry blocks (Bieniasz and Cullen, 2000; Browning et al., 1997). This has led to the development of “humanized mouse” models, such as the bone marrow, liver, thymus (BLT) mouse (Melkus et al., 2006; Wege et al., 2008), comprising immunodeficient mouse strains

¹Infectious Diseases Division, Department of Medicine, Weill Cornell Medical College, New York, NY; ²Immunology & Microbial Pathogenesis Graduate Program, Weill Cornell Graduate School of Medical Sciences, New York, NY; ³Theoretical Biology and Biophysics, Los Alamos National Laboratory, Los Alamos, NM; ⁴Department of Microbiology, Immunology & Tropical Medicine, The George Washington University School of Medicine and Health Sciences, Washington, DC; ⁵PhD Program in Epidemiology, Milken Institute School of Public Health, The George Washington University, Washington, DC; ⁶Center for Cancer and Immunology Research, Children’s National Health System, Washington, DC; ⁷George Washington University Cancer Center, George Washington University, Washington, DC; ⁸British Columbia Centre for Excellence in HIV/AIDS, Vancouver, British Columbia, Canada; ⁹Repertoire Immune Medicines, Cambridge, MA; ¹⁰Ragon Institute of Massachusetts General Hospital, Massachusetts Institute of Technology, and Harvard University, Boston, MA; ¹¹Institute for Medical and Engineering Sciences, Massachusetts Institute of Technology, Cambridge, MA; ¹²Howard Hughes Medical Institute, Chevy Chase, MD; ¹³Faculty of Health Sciences, Simon Fraser University, Burnaby, British Columbia, Canada; ¹⁴Department of Material Science and Engineering, Massachusetts Institute of Technology, Cambridge, MA; ¹⁵Koch Institute for Integrative Cancer Research, Massachusetts Institute of Technology, Cambridge, MA; ¹⁶Department of Biological Engineering, Massachusetts Institute of Technology, Cambridge, MA.

*C.D. McCann, C.H. van Dorp, and A. Danesh contributed equally to this paper; Correspondence to R. Brad Jones: rbrjones@med.cornell.edu.

© 2021 McCann et al. This article is distributed under the terms of an Attribution–Noncommercial–Share Alike–No Mirror Sites license for the first six months after the publication date (see <http://www.rupress.org/terms/>). After six months it is available under a Creative Commons License (Attribution–Noncommercial–Share Alike 4.0 International license, as described at <https://creativecommons.org/licenses/by-nc-sa/4.0/>).

xenografted with human stem cells and/or tissues to generate CD4⁺ T cells that support HIV replication (reviewed in [Marsden and Zack, 2015](#); [Whitney and Jones, 2018](#)). While these models have deepened our understanding of HIV pathogenesis and facilitated therapeutic development ([Denton et al., 2012](#); [Deruaz and Luster, 2013](#); [Halper-Stromberg et al., 2014](#); [Jones et al., 2017](#)), several key factors have substantially limited their utility for the study of HST cells. First, most humanized mouse models, including the BLT mouse, are substantially restricted in terms of possible experimental timelines due to the development of graft-versus-host disease (GvHD), caused by the xenogenic reaction of human cells toward mouse tissues, resulting in severe morbidity and mortality ([Greenblatt et al., 2012](#)). Second, although some HST cell responses can arise in these models, efforts to modulate these through vaccination have met with only limited success ([Dudek et al., 2012](#)). In the cancer field, by contrast, clinical responses to adoptive T cell transfer have been modeled by engrafting immunodeficient mice with patient-derived tumors and subsequently with patient-derived T cell therapy products ([Jespersen et al., 2017](#)). Such approaches would be advantageous for HIV but are not possible using humanized mouse models that are engrafted with fetal cells/tissues, as these do not have a corresponding person from whom to generate autologous T cell therapy products. Ethical considerations around the use of human fetal tissues further underscore the urgent need for alternative mouse models of HIV.

Prior to the development of stem cell/fetal tissue-derived mouse models, early humanized mouse models involved the injection of human peripheral blood mononuclear cells (PBMCs) into CB17-SCID mice ([Mosier et al., 1988](#)). These mice supported HIV infection but were limited by poor and inconsistent levels of engraftment, driven by rejection of human cells by murine natural killer (NK) cells. Engraftment of human PBMCs was dramatically enhanced in the nonobese diabetic severe combined immunodeficiency IL2r γ ^{null} (NSG) mouse (which lacks NK cells; [Spranger et al., 2012](#)), but fatal GvHD occurred particularly rapidly (within 3–4 wk) in hu-PBL-SCID mice. Here, we demonstrate that the engraftment of NSG mice with purified memory CD4⁺ T cells, obtained from individuals with or without HIV, yields mice that support sustained viral replication in this critical cell population that largely harbors the infectious reservoir in humans ([Chomont et al., 2009](#); [Chun et al., 1997](#); [Chun et al., 1995](#); [Finzi et al., 1997](#)) while abrogating GvHD. This parallels studies of allogeneic stem cell transplantation, which have demonstrated that transfusion with only memory CD4⁺ T cells reduces the development of GvHD while still maintaining antigen-specific responses ([Anderson et al., 2003](#); [Huang and Chao, 2017](#)). We establish the utility of this model in evaluating clinically relevant T cell therapy products as well as innovative approaches to enhance these products. We further demonstrate that this model robustly recapitulates T cell epitope escape mutations that are a hallmark of natural HIV infection. This model thus is a valuable tool for studying the evolution of HST cell responses and for evaluating strategies to curb immune escape and establish durable immune-mediated control of HIV replication ([Allen et al., 2005](#); [Jones et al., 2012](#); [McMichael et al., 2010](#); [Patel et al., 2016](#)). Finally, we highlight a notable parallel

between our model and “patient-derived xenograft” (PDX) models of cancer: Both engraft mice with the affected cells from individuals (HIV-infected CD4⁺ T cells and tumor cells, respectively) and subsequently test autologous immune effectors (HST cells and tumor-infiltrating T cells, respectively) along with various adjuvant therapies. As the first PDX model for HIV, we propose the term “HIV PDX mouse model” to emphasize the distinction from human fetal tissue-derived “humanized” mouse models of HIV.

Results

Engraftment with memory CD4⁺ T cells greatly diminishes GvHD compared with total CD4⁺ T cells

In the setting of hematopoietic cell transplantation, the naive T cell compartment is largely responsible for giving rise to the allogeneic reactions that result in GvHD and/or transplant rejection ([Anderson et al., 2003](#); [Chen et al., 2004](#)). This is likely because the naive TCR repertoire is vastly more diverse than the memory TCR repertoire and thus more likely to encompass alloreactive clonotypes ([Anderson et al., 2003](#)). We therefore hypothesized that naive human T cells would drive xenogeneic reactions and GvHD in mice. To evaluate this, we compared GvHD onset and severity in mice engrafted with total CD4⁺ T cells to those engrafted with only the memory subset of CD4⁺ T cells.

Total or memory CD4⁺ T cells were enriched from HIV-negative donor PBMCs via negative selection ([Fig. S1](#)). NSG mice, which lack murine T cells, B cells, and NK cells, were engrafted with 5×10^6 CD4⁺ T cells and bled weekly to quantify and phenotype peripheral CD4⁺ T cells. We observed robust engraftment of CD4⁺ T cells in both groups of mice, though at higher levels in mice that received total CD4⁺ T cells ($P < 0.05$; [Fig. 1 A](#)). In the latter group, this expansion corresponded with increasing proportions of memory CD4⁺ T cells (CD4⁺/CD45RO⁺) and the loss of the naive compartment by 28 d after engraftment ([Fig. 1 B](#)). The onset of GvHD was measured primarily by weight loss, a reliable indicator of acute GvHD in mice ([Fontaine and Perreault, 1990](#)). Mice that received total CD4⁺ T cells began losing weight rapidly ~4 wk after engraftment and died or had to be euthanized by 7 wk after engraftment ([Fig. 1 C](#)). This weight loss was accompanied by observable signs of GvHD, including blepharitis, fur loss, and hunched posture. The onset of GvHD in total CD4⁺ T cell mice was associated with high levels of IFN- γ in blood plasma, indicating the activation of engrafted T cells ([Fig. 1 D](#)). In contrast, mice that had received memory CD4⁺ T cells had ~10 \times lower levels of IFN- γ , in the range of physiological concentrations ([Fig. 1 D](#); [Kleiner et al., 2013](#)). Histology revealed that, while tissue engraftment of CD4⁺ T cells was similar between both groups ([Fig. 1, E and F](#)), mice receiving total CD4⁺ T cells exhibited more severe secondary pathologies according to a blinded pathology report (i.e., perivascular cuffing, apoptosis/necrosis, and multinucleated/syncytial cells; [Fig. 1 E, inset](#)). Thus, the injection of NSG mice with only the memory (CD45RO⁺) subset of CD4⁺ T cells results in robust engraftment while largely avoiding the severe GvHD that rapidly occurs in mice engrafted with total CD4⁺ T cells.

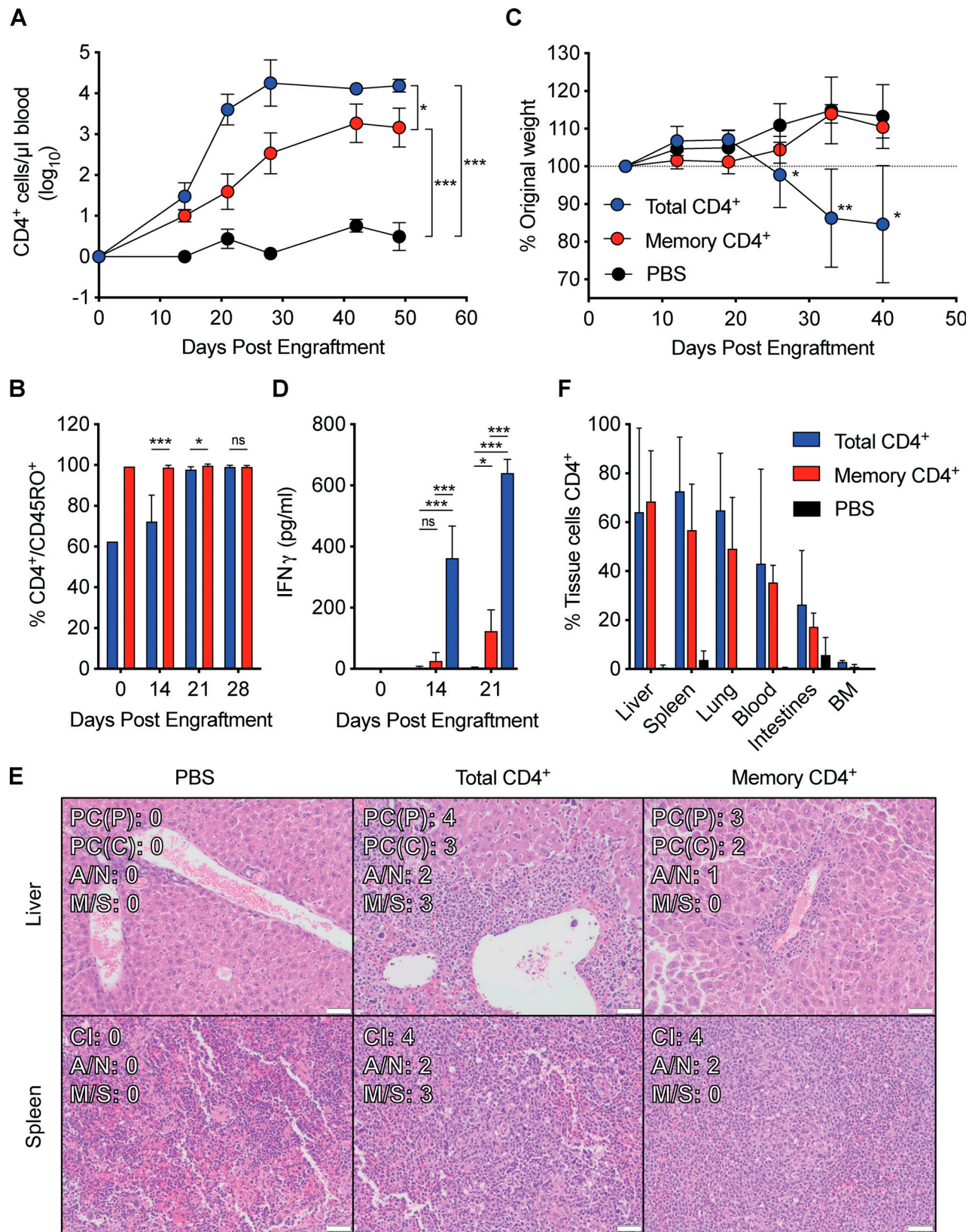


Figure 1. **Engraftment of NSG mice with memory CD4⁺ T cells abrogates the GvHD observed with total CD4⁺ T cells.** (A) Peripheral blood CD4⁺ T cell counts from NSG mice engrafted with total CD4⁺ T cells (*n* = 6), memory CD4⁺ T cells (*n* = 6), or PBS control (*n* = 3), as determined by flow cytometry. (B) Percentages of CD4⁺ T cells with memory phenotypes (CD45RA⁻/CD45RO⁺). Day 0 displays the percentage of cells with memory phenotype from pooled cells before engraftment, while days 14–28 cells were collected from the peripheral blood of mice. (C) Mice were weighed weekly to assess the clinical impact of cell infusion. Data are presented as percentage changes from original weight. (D) Quantification of IFN-γ levels in mouse plasma measured by ELISA.

(E) Representative examples of hematoxylin and eosin-stained cross-sections of spleen and liver tissues. Insets display blinded pathology report values. PC, perivascular cuffing; (P), periportal; (C), centrilobular; A/N, apoptosis/necrosis; M/S, multinucleated/syncytial cells; CI, cellular infiltrate. Scores range from 1 to 4, with 4 being most severe. Scale bars represent 100 μ m. (F) Distributions of CD4⁺ T cells across various tissues 57 d after initial engraftment. BM, bone marrow. All data are expressed as mean \pm SD and considered statistically significant at *, $P < 0.05$; **, $P < 0.01$; ***, $P < 0.001$ using a linear mixed-effects model with Geisser-Greenhouse correction (A) or Student's *t* test (B–D). Results are representative of at least two independent experiments.

Memory CD4⁺ T cell xenograft model recapitulates key features of HIV replication dynamics

We next determined whether memory CD4⁺ T cell-engrafted NSG mice would sustain HIV replication. Five NSG mice were engrafted with 5×10^6 purified memory CD4⁺ T cells each from an HIV-negative donor and infected with HIV_{JR-CSF} at 43 d after engraftment. We observed robust viral replication, which reached a set point of $\sim 10^6$ – 10^7 HIV RNA copies/ml (Fig. 2). This was accompanied by the rapid depletion of peripheral CD4⁺ T cells, mirroring acute infection in humans. At 7 wk after infection, mice were initiated on an ARV drug regimen composed of daily subcutaneous injections of tenofovir disoproxil fumarate (TDF), emtricitabine (FTC), and dolutegravir (DTG). This is the same formulation that has been used to treat rhesus macaques for >1 yr (Borducchi et al., 2018; Whitney et al., 2018), scaled to mice by surface area conversion. ART suppressed HIV replication and allowed CD4⁺ T cell counts to recover, and ART discontinuation reversed these effects (Fig. 2). Thus, this model recapitulates key features of viral replication and CD4⁺ T cell dynamics in untreated (No Tx) and treated HIV infection.

Post hoc power calculations using pooled viral load (VL) data from three independent experiments revealed that a 1- \log_{10} mean difference in VL between two groups at a single time point can be detected with 80% power with five mice per group (Fig. S2). This suggests that this model could be used to ascertain even modest antiviral effects of therapeutic strategies with limited numbers of mice.

IL-15 superagonist (IL-15SA) cell priming enhances proliferation and cytotoxic activity of a CD8⁺ HST cell clone in vitro

A unique advantage of engrafting mice with CD4⁺ T cells from adults is that it offers the opportunity to generate graft-

autologous T cell effectors in vitro and test their antiviral activity in vivo. As has been exploited in various cancer models, the in vitro generation of these T cell products facilitates both engineering of their antigen specificity profiles and modulation of their functional profiles. We therefore designed an experiment to test both of these capabilities. To illustrate precise control of antigen specificity, we analyzed the antiviral activity of an HIV-specific CD8⁺ T cell clone targeting the RLRDLLLIVTR (RR11) epitope in HIV-Env (Fig. S3), which had been expanded from a single cell isolated from participant OM5220 (see Fig. S5). Targeting of RR11 has been associated with relative HIV viremia control, suggesting that such responses may be protective (Pereyra et al., 2014). We engrafted mice with purified memory CD4⁺ T cells from this same individual to allow for in vivo testing of this RR11-specific CD8⁺ T cell clone against autologous target cells.

While CD8⁺ T cell clones offer exquisite antigen specificity, they have historically performed relatively poorly in vivo following adoptive cell therapy, likely due to the lack of CD4⁺ T cell help and of supporting cytokines (Brodie et al., 1999; Koenig et al., 1995; Lieberman et al., 1997). We therefore combined our approach with an innovative strategy designed to enhance the persistence and functionality of adoptively transferred cells through focused delivery of cytokine support. This “cell priming” approach involves the physical loading of effector T cells with “nanogel” (NG) particles (Tang et al., 2018) composed of cross-linked matrices of supporting cytokines—in the current case, an IL-15SA—that releases cytokines over time (Fig. 3 A). This IL-15SA cell priming approach is currently in a phase 1 clinical trial for relapsed/refractory solid tumors and lymphomas (NCT03815682). Enhancements of CD8⁺ T cell proliferation and cytotoxic activity by IL-15SA have also been observed

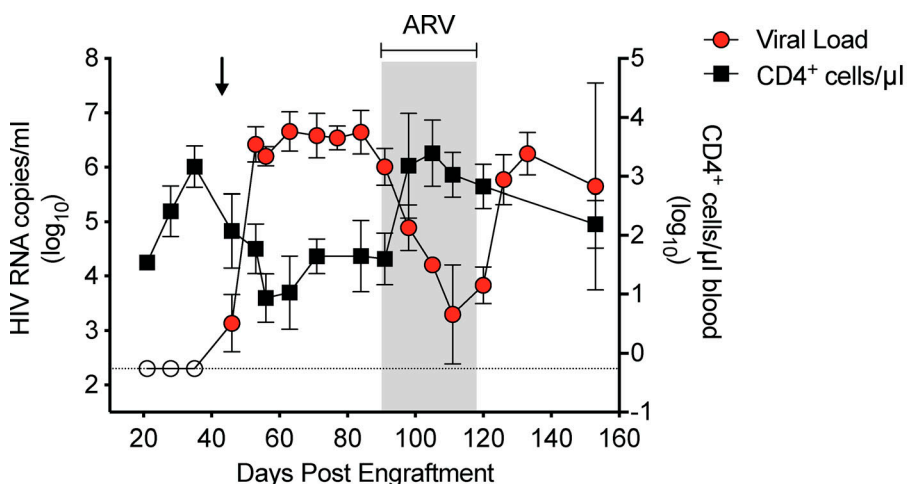


Figure 2. **Memory CD4⁺ T cell-engrafted mice recapitulate features of natural and treated HIV infection.** NSG mice ($n = 5$) were engrafted with 5×10^6 memory CD4⁺ T cells isolated from an HIV-negative donor. Mice were bled weekly, and VL (red circles; left axis) and CD4⁺ T cells (black squares; right axis) are presented. 43 d after engraftment, mice were infected with 100,000 TCID₅₀ HIV_{JR-CSF} (arrow). 90 d after engraftment, mice were started on a daily regimen of s.c. administered ARV cocktail consisting of 57 mg/kg TDF, 143 mg/kg FTC, and 7 mg/kg DTG (shaded region). ART was stopped at 118 d after engraftment. HIV RNA limit of detection = 200 copies (dashed horizontal line), sample averages below limit of detection represented as open circles. Data are expressed as mean \pm SD. Results shown are representative of more than three independent experiments.

in HIV (Jones et al., 2016; Mota et al., 2020). Therefore, we sought to determine if the enhancing effects of IL-15SA cell priming on cancer-specific CD8⁺ T cells would translate to HIV-specific CD8⁺ T cells in our PDX model.

We began by optimizing the IL-15SA NG loading conditions for this CD8⁺ T cell clone and studied the impact of this on proliferation and effector function in vitro. RR11-specific CD8⁺ T cells were incubated with IL-15SA-containing NG over a range of concentrations resulting in surface-bound IL-15SA, as determined by flow cytometry (IL-15⁺/IgG⁺; Fig. 3 B). Surface staining for IL-15SA was absent by 24 h (Fig. 3 B) due to a positive charge of the NG inducing endocytosis (Behzadi et al., 2017) and the cytokine-induced receptor-mediated internalization, as seen previously (Tang et al., 2018). A dose-dependent expansion of IL-15SA priming of RR11-specific CD8⁺ T cells was observed in vitro, with the highest concentration (1.5 mg/ml) showing an eightfold increase in cell numbers after 8 d in culture (Fig. 3 C). IL-15SA cell priming also enhanced killing of RR11 peptide-loaded CD4⁺ T cells ($P < 0.001$ at 1:5 effector/target ratio; Fig. 3 D).

Targeted delivery of IL-15SA enhanced antiviral effects of CD8⁺ HST cells in vivo

We next tested the in vivo antiviral activities of unmodified and IL-15SA-loaded RR11-specific CD8⁺ T cells in the HIV PDX mouse model. Mice were engrafted with memory CD4⁺ T cells from study participant OM5220 (autologous to the RR11-specific CD8⁺ T cell clone), infected with HIV_{JR-CSF}, and received adoptive cell transfer of the RR11-specific CD8⁺ T cell clone alone (RR11), IL-15SA NG-loaded RR11 (RR11-NG), or RR11 plus systemic soluble IL-15SA administered at 0.2 mg/kg over three weekly doses (RR11 + IL-15SA; Fig. 4 A). This dose was selected based on previous reports that 0.2 mg/kg of a similar IL-15SA molecule enhanced CD8⁺ T cell and NK cell activity against tumors while avoiding toxicity (Liu et al., 2018; Rhode et al., 2016). After reaching nearly identical peaks, mice receiving RR11-NG showed transient reductions in VL relative to No Tx mice, with the greatest differential observed ~4 wk after adoptive cell transfer (day 49; $P = 0.031$; Fig. 4, B and C). A second administration of RR11-NG was given on day 84, and it again drove a reduction in VL relative to No Tx mice, but not significantly (Fig. 4 B). In contrast, mice that received systemic soluble IL-15SA (as well as RR11-specific CD8⁺ T cells) reached higher peak viremia and sustained a higher viral set point than all other groups. This was likely because systemic IL-15SA induced CD4⁺ T cell activation, as evidenced by high levels of the activation markers CD25 and CD69 in this group ($P < 0.001$ and $P = 0.011$, respectively; Fig. 4 D). No significant differences were observed between the VLs of mice that had received RR11-specific CD8⁺ T cells without IL-15SA and those of No Tx mice.

Overall, our results indicate that infusion of a single HIV-specific CD8⁺ T cell clone in the PDX model was not sufficient to reduce VLs, in line with previous studies of such clones in humans and in nonhuman primate (NHP) models (Bolton et al., 2010; Brodie et al., 1999; Koenig et al., 1995; Lieberman et al., 1997; Minang et al., 2010). Our results do however illustrate the value of this PDX model in assessing strategies to enhance T cell immunotherapies: Whereas soluble and IL-15SA NG supported

similar levels of expansion of CD8⁺ HST cells in vitro (Fig. 3 C), only the targeted NG delivery facilitated a net benefit in terms of in vivo antiviral activity.

Polyclonal HST cells from controller exhibit potent in vivo antiviral activity in PDX mice

The HIV PDX mouse offers the potential to test clinically relevant T cell therapy products against autologous cells in vivo. Toward this goal, we assessed the in vivo antiviral efficacy of a polyclonal, multiepitope-specific T cell product, termed “HST cells” (Patel et al., 2020; Ren et al., 2020), that was anticipated to show superior persistence and efficacy relative to T cell clones based on clinical trial data (Leen et al., 2006; Saglio et al., 2014). HST cells were generated using the same good manufacturing practice-compliant protocol used to generate the analogous T cell products that are being studied in participants with HIV in a clinical trial (NCT03485963). Briefly, HST cells are expanded by co-culturing isolated PBMCs with autologous dendritic cells preloaded with HIV peptide pools spanning HIV Gag, Pol, and Nef (Fig. S3 B; Lam et al., 2015). For the current study, HST cells were generated from participant CIRC0196 (Fig. S5), who expresses HLA-B*5801, an allele associated with enhanced viral control (Fellay et al., 2007; Kiepiela et al., 2004; Migueles et al., 2000). In vitro characterization of these HST cells revealed specificity for multiple T cell epitopes across Gag, Pol, and Nef, including the HLA-B*58-restricted TSTLQEIQIW (TW10; Gag) and QATWIPEWEF (QF10; Pol) epitopes (Fig. S3, C and D). These T cells were polyfunctional, demonstrating secretion of IFN- γ , MIP-1 β , and TNF- α , and effectively lysed peptide-pulsed cells in a chromium release assay (Fig. S3, E and F). As HST cells are generated by co-culturing PBMCs, rather than purified CD8⁺ T cells, with dendritic cells, they also contain minority cell populations with potential effector activity (i.e., NK and NK T cells), but notably lack CD4⁺ T cells (Patel et al., 2018; Patel et al., 2020).

PDX mice were generated as described above, using purified memory CD4⁺ T cells from participant CIRC0196 (autologous to HST cells). 3 wk after engraftment, they were simultaneously infected with HIV_{JR-CSF} by i.p. injection and received adoptive cell transfer by i.v. injection of 5×10^6 autologous, ex vivo expanded HST cells, IL-15SA NG-loaded HST cells (HST-NG), or CMV-specific T cells (CMV) as a negative control, and they were compared with a No Tx group (Fig. 5 A). IL-15SA cell priming was performed as for the CD8⁺ HST cell clone, with 1.5 mg/ml IL-15SA-containing NG. All mice ($n = 30$) displayed rapid viral expansion reaching nearly identical mean VLs 1 wk after infection/T cell injection (Fig. 5 B). Mice in the No Tx and CMV groups sustained high VLs throughout the experiment and displayed marked depletion of peripheral CD4⁺ T cells. In contrast, six of seven (85.7%) mice that received HST cells and seven of seven (100%) mice that received HST-NG showed substantial, yet transient, viral suppression (see Tables 1 and 2 for statistical analyses). Viral suppression in the HST and HST-NG mice was associated with significantly reduced CD4⁺ T cell depletion in the peripheral blood ($P < 0.001$; Fig. 5 B). Viral suppression kinetics also corresponded with the dramatic expansion of peripheral blood CD8⁺ T cells in both the HST and HST-NG groups. This expansion of CD8⁺ T cells was greater than that observed in the

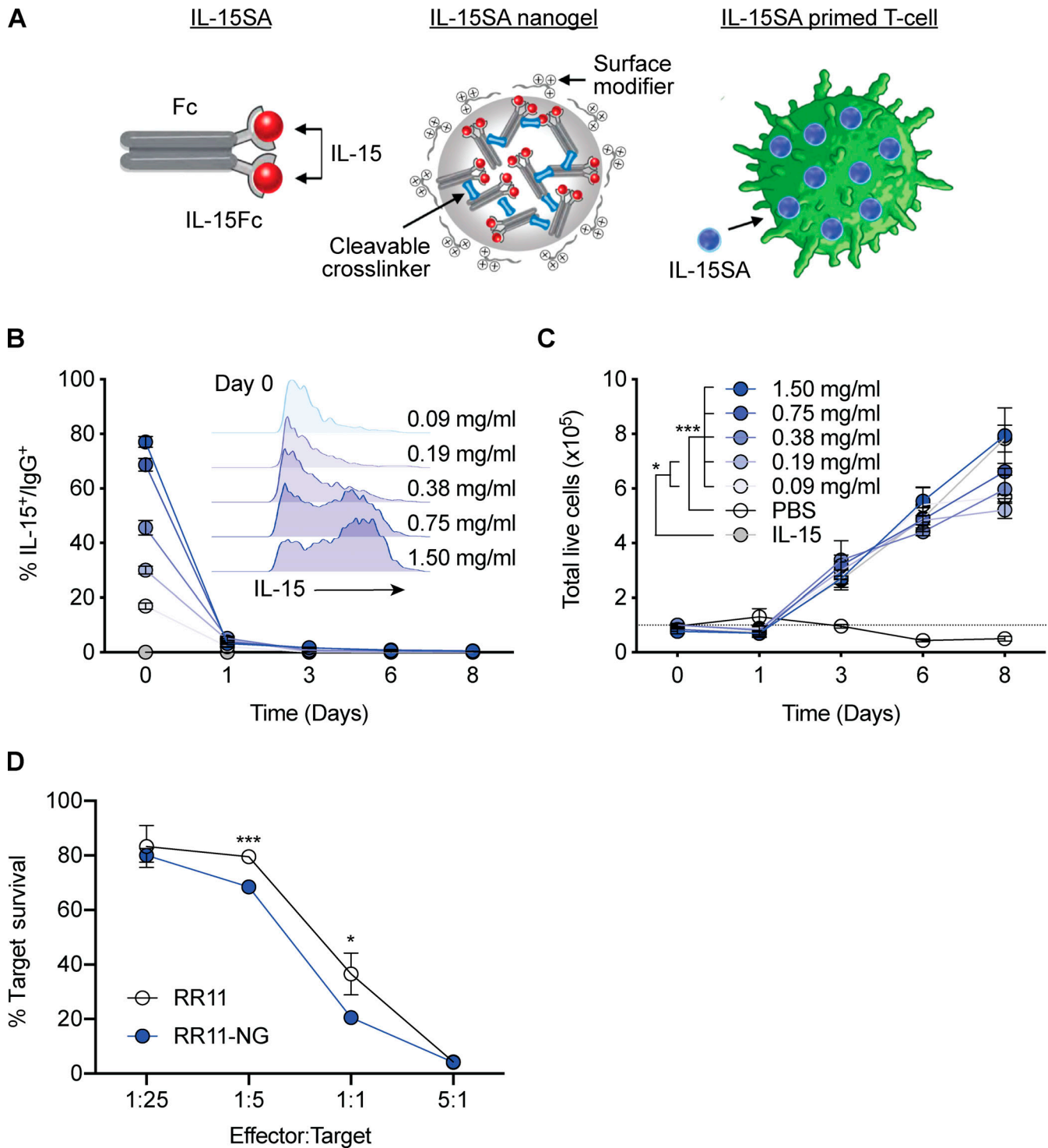


Figure 3. **IL-15SA cell priming enhances expansion and functionality of CD8⁺ HST cell clone in vitro.** (A) Schematic representation of IL-15SA priming of T cells. IL-15SA was generated by noncovalently bonding IL-15 cytokine with IL-15Ra fused to IgG-Fc domain. IL-15SA-containing NGs were formed with cleavable cross-linkers and bound to the plasma membrane of T cells via electrostatic interactions. (B) Shown are flow cytometric analyses of NG-loaded CD8⁺ T cells displaying percentage of cells positive for surface staining of both hu-IL-15 and hu-IgG. Inset depicts histograms of hu-IL-15-positive cells after 1-h incubation with IL-15SA-containing NG at increasing concentrations (day 0). (C) Dose response of CD8⁺ T cell expansion in vitro when augmented with IL-15SA at increasing concentrations or cultured in media supplemented with 50 IU/ml soluble IL-15 or PBS negative control. (D) In vitro killing assay of CD4⁺ T cells pulsed with HIV RR11 peptide and co-cultured overnight at increasing effector-to-target ratios with autologous RR11-specific CD8⁺ T cell clone with and without IL-15SA augmentation (1.5 mg/ml). Each condition was run in triplicate wells. Data are presented as the percentage survival of CD4⁺ T cells determined by amine-reactive cell viability dye staining and flow cytometric analysis. Data are expressed as mean ± SD and considered statistically significant at *, P < 0.05; ***, P < 0.001 using Student's t test. Results shown are representative of two independent experiments.

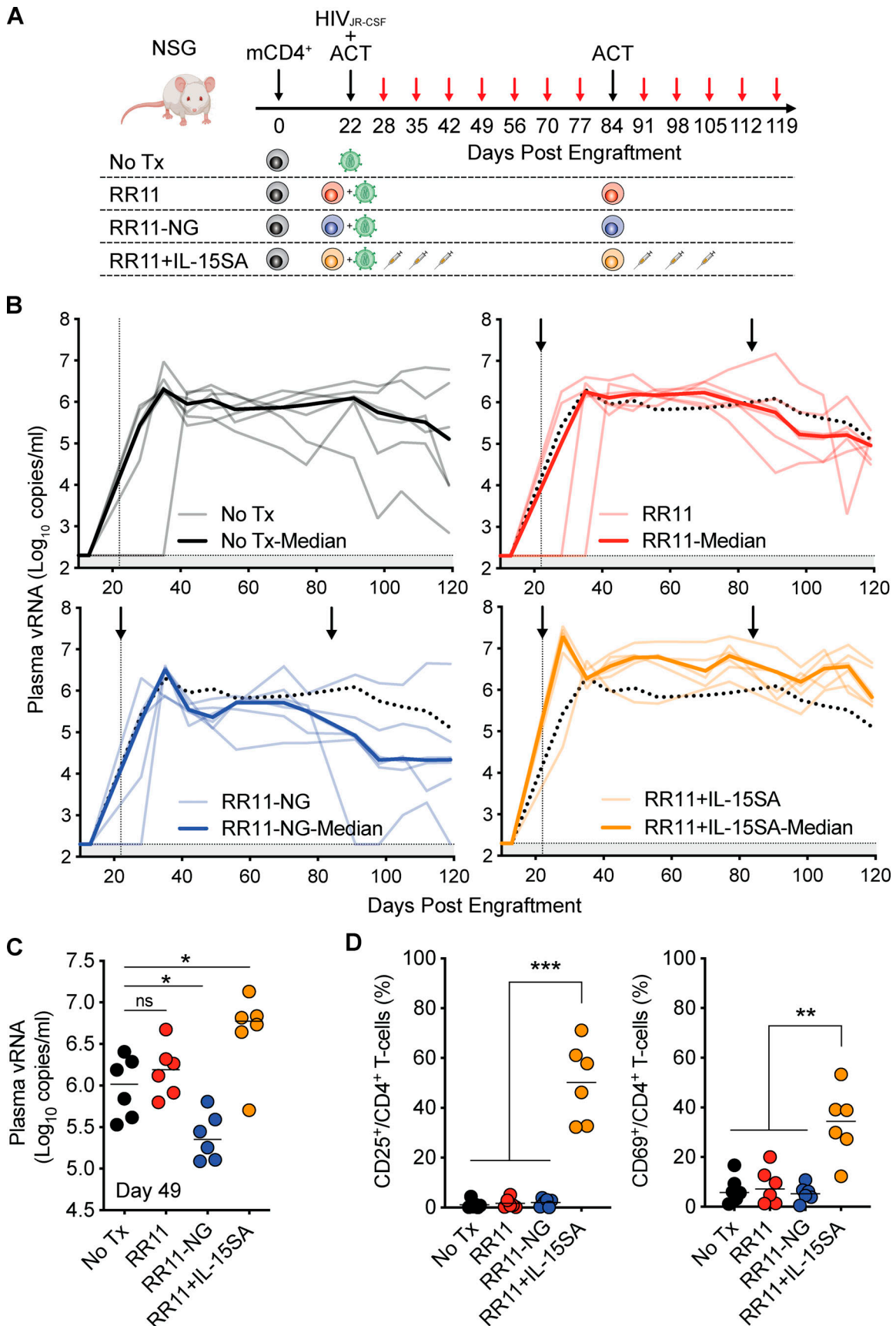


Figure 4. Cell priming targets IL-15SA to CD8⁺ HST cell clone in vivo, enabling antiviral activity while avoiding generalized immune activation. (A) Schematic of in vivo experimental timeline. NSG mice were engrafted with 5×10^6 memory CD4⁺ T cells from an HIV-positive donor (OM5220). 22 d after

engraftment, mice were infected with 100,000 TCID₅₀ HIV_{JR-CSF} (dotted vertical line) by i.p. injection and received adoptive cell transfer (ACT) by i.v. injection of 5×10^6 autologous, RR11-specific CD8⁺ T cell clones ($n = 6$), IL-15SA NG-loaded RR11 clones ($n = 6$), RR11 clones + 0.2 mg/kg systemic administration of IL-15SA ($n = 6$), or No Tx control ($n = 6$). Mice were bled weekly, plasma was analyzed by quantitative RT-PCR for HIV RNA, and cells were stained for flow cytometric analysis. **(B)** Quantification of plasma viral RNA (vRNA; log₁₀ copies/ml) in mice was determined by qRT-PCR. Assay limit of detection = 200 copies/ml (dotted horizontal line). Thin colored lines denote individual mice; thick colored lines denote group median. No Tx group median is displayed across treatment group plots as a thick dotted line for comparison. Arrows denote adoptive cell transfer of CD8⁺ T cells or appropriate controls. **(C)** Comparison of plasma vRNA between treatment groups at day 49 after engraftment (4 wk after adoptive cell therapy). **(D)** Flow cytometric analysis of peripheral blood CD4⁺ T cells expressing surface activation markers CD25 (left) and CD69 (right) at day 28 after engraftment. Bars display group median. Data were analyzed using a linear median mixed-effects model corrected for multiple comparisons (B) or a Mann-Whitney *U* test (C and D). Statistical significance is denoted as *, $P < 0.05$; **, $P < 0.01$; ***, $P < 0.001$. Results shown are representative of two independent experiments.

mice that received CMV-specific T cells, consistent with HIV antigen-driven expansion. Despite sustained high levels of CD8⁺ HST cells in peripheral blood, viral control was not maintained, and all mice that received HIV-specific cell therapy returned to viral set point by 5 wk after HST injection (Fig. 5 B).

Xenograft model recapitulates natural CD8⁺ T cell-driven viral escape mutations

To investigate whether transient viral suppression was attributable to immune escape, we deep sequenced viral RNA at four time points spanning viral suppression and subsequent rebound (days 49, 56, 63, and 70). Sequencing focused on *gag*, as CD8⁺ T cell responses to this gene product associate with viral control (Kiepiela et al., 2007). Sequences largely matched the challenge HIV_{JR-CSF} virus, with the striking exception of substitutions at positions HXB2-Gag 242 and 248. These encode positions 3 and 9 of the well-characterized HLA-B*57/58-restricted TSTLQE-QIGW₂₄₀₋₂₄₉ (TW10) epitope, which elicits an immunodominant and sometimes protective response in HLA-B*57/58⁺ humans (Miura et al., 2009). Epitope mapping of the HST product revealed a TW10 response (Fig. S3 D) that was confirmed by MHC tetramer staining and by ELISPOT with the optimal peptide (Fig. 8 A). Representative sequencing results are provided in Fig. 6 A. At 70 d after engraftment, 85.7% (six of seven) of the mice in the HST group and 100% (seven of seven) of the mice in the HST-NG group harbored mutations in the TW10 epitope compared with 0% (zero of eight) mice in the No Tx group (Fig. 6 B). These included several well-characterized TW10 escape mutations (T242N, G248A, G248E, and G248R) as well as a novel, putative escape mutation (G248K). G248E and G248R appeared earlier and in a greater proportion of mice, whereas T242N, G248A, and G248K appeared later and less commonly (Fig. 6 C). Overall, sequencing revealed considerable heterogeneity in the escape profiles of individual mice, despite their engraftment with the same pool of CD4⁺ T cells, infection with the same molecular clone of HIV_{JR-CSF}, and treatment with the same T cell product. Thus, this model presents a unique opportunity for studying factors governing the dynamics of HIV epitope escape in a controlled scenario.

Loss of immune control results from a combination of viral escape and contraction of the CD8⁺ T cell population

The emergence of CD8⁺ T cell escape mutations is consistent with VL rebound after an initial nadir around day 56 after engraftment. However, not all mice exhibited a high proportion of escaped sequences. Additionally, CD8⁺ T cell concentrations

began to decline after reaching a peak around day 49 (Fig. 5 B), which could have allowed nonescaped viruses to expand. To better identify the causes of rebound, we mathematically modeled the dynamics of WT and mutant virus populations. Full details of the mathematical model are provided in the Materials and methods. In short, we extended the standard viral dynamic model (Perelson, 2002; Perelson and Ribeiro, 2013) by including a CD8⁺ T cell response and separated the population of infected cells into those infected by WT and mutant viruses (Fig. 7 A; Ganusov et al., 2013; Yang and Ganusov, 2018). Motivated by the CD8⁺ T cell data and previous models of antigen-driven T cell expansion in virally infected mice (Althaus et al., 2007), we modeled the CD8⁺ T cell dynamics using an expansion phase followed by contraction to a steady state (De Boer et al., 2001). We assumed that the cells infected by WT virus are killed by the CD8⁺ T cells in a saturated manner and that cells infected by the escape mutant cannot be recognized. We also allowed for the possibility of a fitness cost of escape.

We fit the model using a nonlinear mixed-effects framework to the VL, CD8, and TW10 escape mutation data (Fig. 7 A). An escape mutation was defined as any substitution in either position 3 or 9 of the TW10 epitope. We tested whether any of the model parameters are affected by the treatment type (No Tx, HST, HST-NG, or CMV), and found statistical evidence for a treatment effect on the parameters governing the CD8⁺ T cell dynamics (see Fig. S4 A). Most notably, the model suggests that cell priming with the IL-15SA NG results in a 74% smaller average contraction rate compared with unmodified HST cells, while the expansion phase was, on average, 3.3 d shorter. Interestingly, the IL-15SA NG did not have an effect on the killing rate parameter (Fig. S4 A), suggesting that the beneficial effects of cell priming in this model are due to enhanced survival of the CD8⁺ T cells. During the peak of the immune response (~50.5 d after engraftment), the death rate of an infected cell (with WT virus) was increased by 2.2 d⁻¹ (interquartile range, 2.0–2.3 d⁻¹).

We identified three scenarios that explain the VL kinetics and escape mutant frequencies observed in different mice. In the first scenario (Fig. 7 B, minor escape), CD8⁺ T cell expansion initially reduced VLs via killing of infected cells. The escape mutant then appeared at a small frequency, but before the mutant became dominant, the CD8⁺ T cell population had already contracted. The WT virus thus remained dominant due to lack of immune pressure or the fitness cost of escape. In the second scenario (Fig. 7 B, transient), CD8⁺ T cell expansion was more profound and led to an initial VL decline, but due to increased selection pressure, the escape mutant grew rapidly,

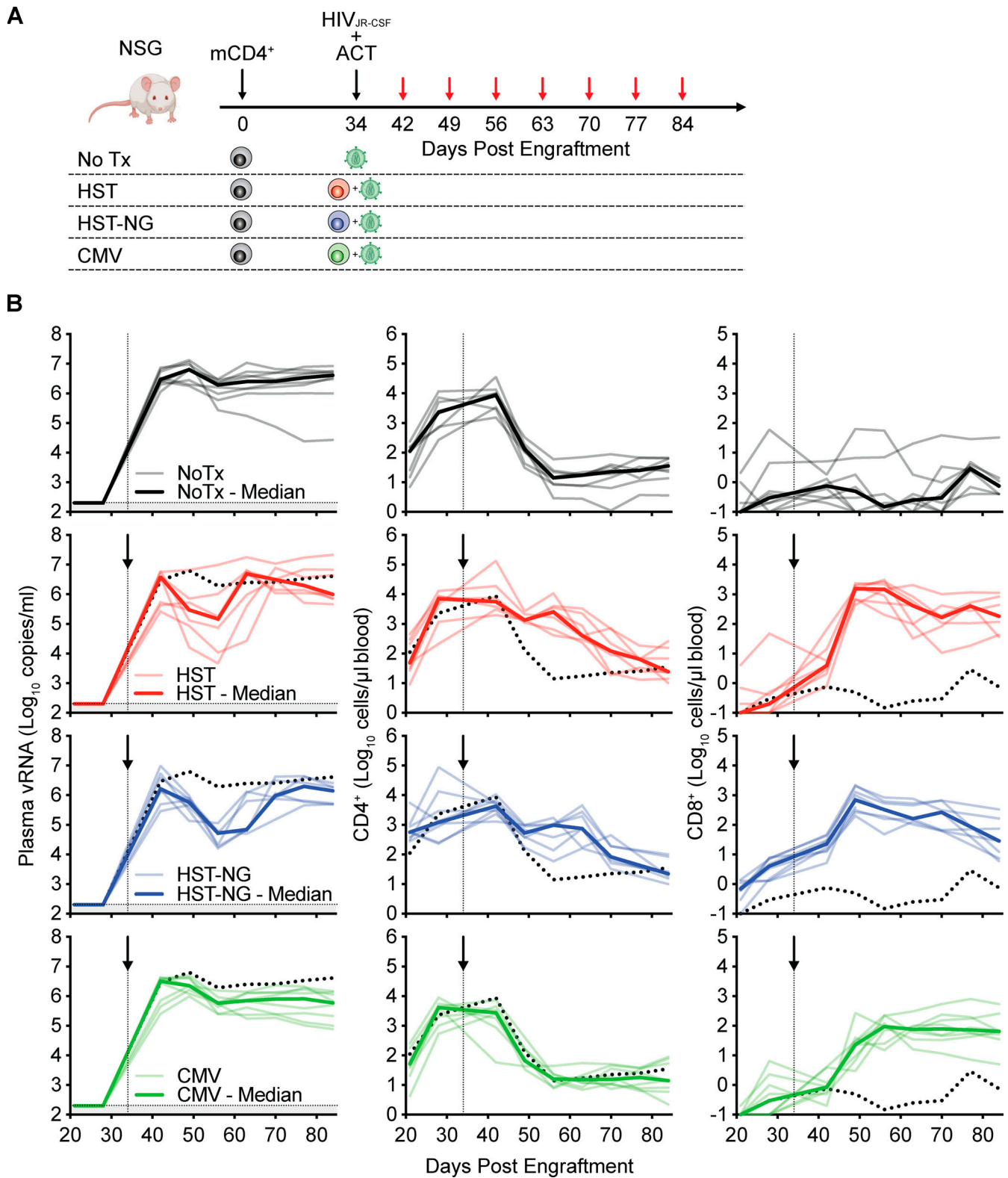


Figure 5. **A clinically relevant ex vivo expanded HST cell product displays potent in vivo antiviral activity, which is further enhanced by IL-15SA.** **(A)** Schematic of experimental timeline. NSG mice were engrafted with 5×10^6 memory CD4⁺ T cells from an HIV-positive donor (CIRC0196). 5 wk after engraftment, mice were infected with 100,000 TCID₅₀ HIV_{JR-CSF} and received infusions of 5×10^6 autologous HST cells ($n = 7$), IL-15SA primed HST cells ($n = 7$), CMV-specific CD8⁺ T cells ($n = 8$), or No Tx control ($n = 8$). Mice were bled weekly, plasma was analyzed by quantitative RT-PCR for VL, and cells were stained for flow cytometry. **(B)** Quantification of HIV plasma viral RNA (left), CD4⁺ T cells (center), and CD8⁺ T cells (right) in peripheral blood of xenograft mice collected over weekly intervals. Thin colored lines represent individual mice; thick colored lines represent group medians. Vertical dashed line indicates time of HIV_{JR-CSF} infection, and arrows denote time of adoptive cell transfer. The limit of detection for the qRT-PCR VL assay was 200 copies/ml (horizontal dashed line and shaded region). No Tx group median displayed across treatment group is plotted as a thick dotted line for comparison. Longitudinal data were analyzed using a linear median mixed-effects model corrected for multiple comparisons. Results shown are representative of three independent experiments.

Table 1. **Viral load linear median mixed-effects model group comparisons**

Group comparison	Estimate ^a	P value ^b
CIRC0196 (Fig. 5) full model^c: days 42–84 after engraftment		
No Tx vs. CMV	0.39	0.228
No Tx vs. HST	0.34	0.346
No Tx vs. HST-NG	0.52	0.046
CIRC0196 (Fig. 5) restricted model^d: days 42–56 after engraftment		
No Tx vs. CMV	0.37	0.061
No Tx vs. HST	0.94	0.005
No Tx vs. HST-NG	0.75	<0.001
WWH004 (Fig. 8) full model^c: days 51–99 after engraftment		
No Tx vs. CMV-NG	0.36	0.504
No Tx vs. HST-NG	0.80	0.170
WWH004 (Fig. 8) restricted model^d: days 51–65 after engraftment		
No Tx vs. CMV-NG	0.26	0.603
No Tx vs. HST-NG	0.31	0.538

^aEstimate comparing log₁₀-transformed VLs between groups.

^bAdjusted for multiple comparisons using multivariate *t*-distribution method. Bolded P value denotes significance.

^cModeling longitudinal VLs from peak viremia to end of study.

^dModeling longitudinal VLs from peak viremia to point of viral escape.

leading to viral rebound beginning around day 55. As soon as the CD8⁺ population contracted, however, the fitness cost of escape caused the WT to outcompete the mutant, and the mutant frequency declined. The third scenario (Fig. 7 B, fixation) began as the second scenario did, but now the CD8⁺ population contracted to a steady state in which enough immune pressure was maintained to cause the mutant to take over completely, despite the fitness cost. In all scenarios, we estimated that, on average, a TW10 escape mutation reduced viral fitness by 56% (interquartile range, 50–62%). The HIV PDX mouse model is unique in that it allows the study of how different patterns of escape mutations, along with viral and cellular dynamics, emerge despite homogeneous starting conditions (where mice are engrafted with the same pool of CD4⁺ T cells, infected with the same molecular clone of HIV_{JR-CSF}, and treated with the same T cell products). By applying mathematical modeling, we show that the kinetics and timing of the CD8⁺ response profoundly impacted the emergence and persistence of CD8⁺ escape mutations, a conclusion that has been surprisingly difficult to reach with human data (Yang and Ganusov, 2018).

Antiviral activity in PDX mice tracks with pre-injection exhaustion of epitope-specific CD8⁺ T cells

Comparative studies of individuals who naturally control HIV replication, versus those who do not, have emphasized qualitative rather than quantitative features of effective CD8⁺ T cell responses, including proliferative capacity and low expression of mediators of T cell exhaustion, primarily PD-1 (Day et al., 2006; Jones et al., 2008; Petrovas et al., 2006; Trautmann et al., 2006). As an initial assessment of whether this is recapitulated in the PDX mouse model, we performed an experiment matched to that shown in Figs. 5, 6, and 7 (donor CIRC0196)

using cells from a second HLA-B5801⁺ donor (WWH004). Whereas CIRC0196 had achieved partial control of viremia before ART initiation (Fig. S5), WWH004 had progressive disease and was diagnosed with AIDS following hospitalization, with a CD4 count <200 cells/mm³. Likely as a reflection of these histories, although the HST product from WWH004 had a higher magnitude of TW10-specific T cell responses by IFN- γ ELISPOT than that of CIRC0196 (and a similar profile of responsiveness to the epitope variants selected by CIRC0196 in mice; Fig. 8 A), MHC-I tetramer staining showed these to be PD-1^{hi} in WWH004 versus PD-1^{low} in CIRC0196 and to express higher levels of perforin in WWH004 (Fig. 8, B and C). Corresponding with PD-1 expression levels, TW10-specific CD8⁺ T cells from CIRC0196 proliferated vigorously in vitro in response to peptide, while those from WWH004 showed only minimal proliferation. All T cell products from WWH004 were conjugated to IL-15SA NGs before injection, based on the augmentation observed with this approach for CIRC0196. In PDX mice, HST-NGs from WWH004 showed little to no antiviral activity (not statistically significant; Fig. 8 F; Table 1 and Table 2), without protection from CD4 depletion. Although in vivo expansion of CD8⁺ T cells occurred in the HST-NG-treated mice, and to a greater degree than in mice treated with CMV-NG (Fig. 8 F), this was substantially slower, and muted in magnitude, relative to that observed in HST or HST-NG treated mice with CIRC0196.

Also, in contrast to CIRC0196, sequencing revealed a paucity of escape mutations for WWH004, with only the following cases in the HST-NG group showing sequence variation at >1% prevalence at day 78: Two of eight mice in the HST-NG group showed the G248R mutation at 2.5% and 4.5%. A comprehensive examination of the degree to which the PDX mouse consistently recapitulates control of viremia from corresponding donors will

Table 2. Viral load comparisons at individual time points

CIRC0196 (Fig. 5)			WWH004 (Fig. 8)		
Group comparison	Mean difference^a	Adjusted P value^b	Group comparison	Mean difference^a	Adjusted P value^b
Day 42 (1 wk after infection)			Day 51 (1 wk after infection)		
No Tx vs. CMV	0.291	0.424	No Tx vs. CMV-NG	0.160	0.946
No Tx vs. HST	0.293	0.574	No Tx vs. HST-NG	-0.011	1.000
No Tx vs. HST-NG	0.255	0.549			
Day 49			Day 58		
No Tx vs. CMV	0.354	0.106	No Tx vs. CMV-NG	-0.286	0.745
No Tx vs. HST	1.271	0.015	No Tx vs. HST-NG	-0.212	0.837
No Tx vs. HST-NG	1.036	<0.001			
Day 56			Day 65		
No Tx vs. CMV	0.396	0.085	No Tx vs. CMV-NG	0.458	0.600
No Tx vs. HST	0.991	0.161	No Tx vs. HST-NG	0.845	0.167
No Tx vs. HST-NG	1.550	<0.001			
Day 63			Day 72		
No Tx vs. CMV	0.525	0.115	No Tx vs. CMV-NG	0.708	0.549
No Tx vs. HST	0.086	0.995	No Tx vs. HST-NG	1.024	0.307
No Tx vs. HST-NG	1.004	0.023			
Day 70			Day 79		
No Tx vs. CMV	0.463	0.274	No Tx vs. CMV-NG	0.545	0.544
No Tx vs. HST	-0.252	0.709	No Tx vs. HST-NG	0.867	0.264
No Tx vs. HST-NG	0.244	0.775			
Day 77			Day 85		
No Tx vs. CMV	0.499	0.418	No Tx vs. CMV-NG	0.143	0.964
No Tx vs. HST	-0.147	0.964	No Tx vs. HST-NG	0.537	0.625
No Tx vs. HST-NG	0.085	0.991			
Day 84					
No Tx vs. CMV	0.676	0.183			
No Tx vs. HST	0.004	1.000			
No Tx vs. HST-NG	0.284	0.743			

^aMean difference in log₁₀-transformed VLs.

^bBrown-Forsythe and Welch ANOVA test with Dunnett's multiple comparison test. Bolded P value denotes significance.

require further experimentation. The current study provides an impetus for this additional direction for the model by showing that T cells from different donors targeting the same epitope in the same viral clone (HIV_{JR-CSF}) can manifest very different in vivo antiviral activities in the PDX mouse and that this corresponded with phenotypic (Fig. 8, B and C) and functional (Fig. 8 E) features associated with natural control in humans (Day et al., 2006; Horton et al., 2006; Migueles et al., 2002; Petrovas et al., 2006; Trautmann et al., 2006).

Discussion

The well-established role that T cell responses play in naturally occurring cases of immunological control provides a strong rationale for the development of T cell-based HIV therapies.

However, a paramount obstacle to realizing this potential has been the need to develop strategies that counter the ability to escape cellular immune responses via mutation (Gaiha et al., 2019). An analogous challenge exists for HIV-specific antibody-based therapies, though broadly neutralizing antibodies (bNAbs; reviewed in Caskey et al., 2019) now represent at least a partial solution. The evaluation and development of bNAbs has benefited greatly from innovations in animal models, including the ability to infect NHPs with chimeric simian immunodeficiency virus/HIV ("SHIV") viruses that incorporate HIV's envelope protein and thus recapitulate its bNAb susceptibility characteristics. Numerous studies have leveraged this platform to study antibody escape kinetics and strategies to block this, including through bNAb combinations (Julg et al., 2017; Nishimura et al., 2017). The development of CD8⁺ T cell-based

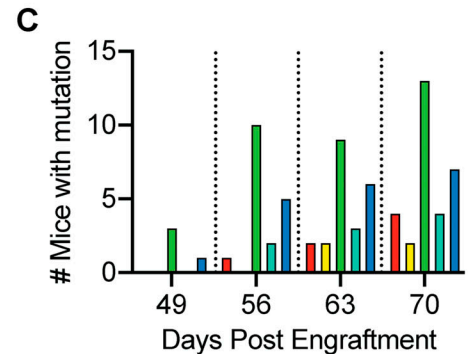
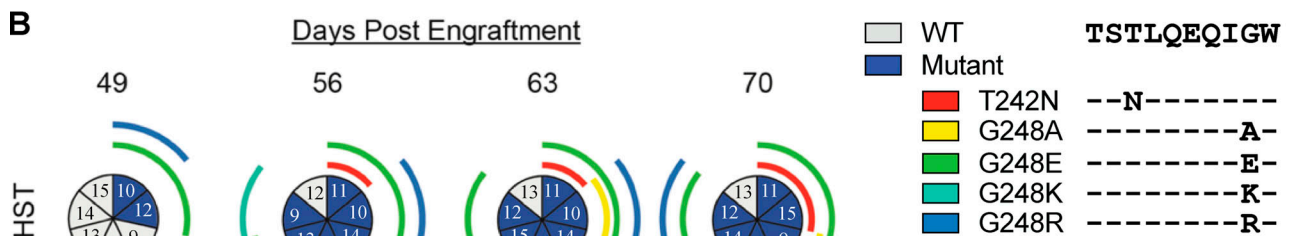
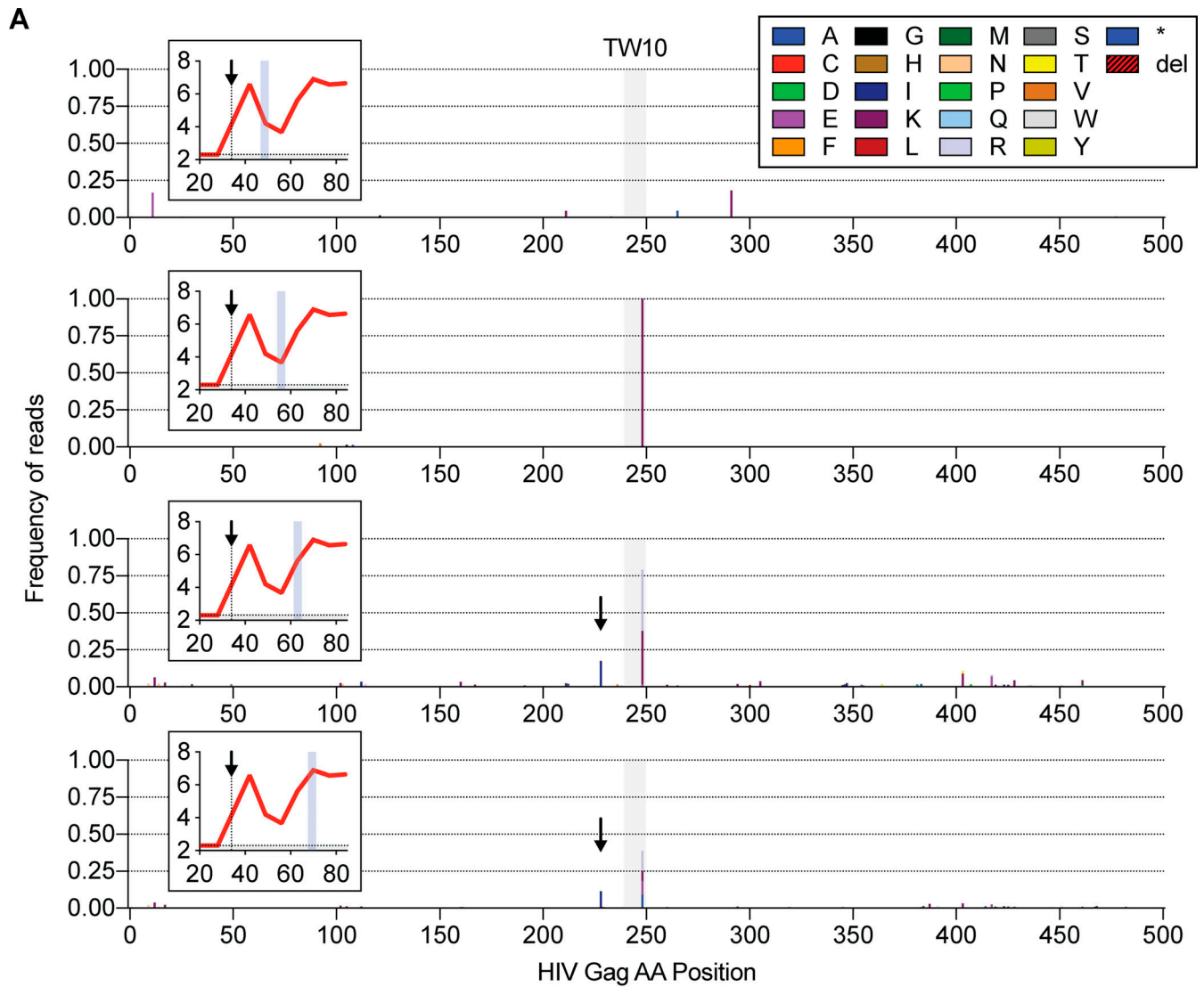


Figure 6. HST cells drive high levels of escape mutations, which exhibit diverse patterns across HIV PDX mice. **(A)** Representative graphs of *gag* deep sequencing of plasma RNA from one mouse (HST group) across four time points (days 49, 56, 63, and 70). Bars represent the frequency of sequencing reads that differ from the clonal HIV_{JR-CSF} inoculation sequence, colored by the substituting amino acid (*, insertion; del, deletion). Insets display the corresponding VL graph (y axis, HIV RNA log₁₀ copies/ml; x axis, days after engraftment) with the analyzed time point highlighted (light blue). Light gray shaded region highlights the HLA-B*57/58–restricted TSTLQEQIGW (TW10) epitope of Gag. The arrows identify the M228I compensatory mutation near the cyclophilin A binding loop of HIV capsid. **(B)** Pie charts depicting the frequencies of mice with TW10 escape mutations (blue segments), comparing the HST (top row) and HST-NG (bottom row) treatment groups across four time points. Numbers indicate mouse identifiers and correspond with those in Fig. S4. The presence of escape mutation was defined as >1% of sequencing reads. No mutations above this threshold were observed in the No Tx group. Outer rings indicate specific amino acid mutations. **(C)** Bar charts displaying the total numbers of mice (HST and HST-NG groups combined) with indicated TW10 variants over time. Results shown are representative of two independent experiments.

therapies has suffered from the lack of an analogous solution, leaving a critical gap between the existing wealth of human data implicating associations between specific epitopes and HIV control and the lack of an ability to test the elicitation of responses to these particular epitopes in an NHP model (due to differences in both the virus and host MHC-I). Our principal aim in developing this model was to facilitate the development of T cell therapies for HIV toward realizing their potential to enable durable control of HIV replication. This development will be timely, as it will enable the HIV field to leverage the rapid advances in natural and engineered immunotherapies that continue to revolutionize cancer therapy. The study of such approaches in HIV PDX mice may, in turn, provide insights that inform further development in cancer. For example, by leveraging the extraordinarily dynamic readout of HIV VL, which lends itself to mathematical modeling, we provide evidence that IL-15SA cell priming acts by slowing the contraction of CD8⁺ T cells rather than enhancing killing on a per-cell basis.

A unique aspect of the HIV PDX model is that the same T cell products being administered to clinical trial study participants can be tested in mice. Thus, this model can be highly personalized and may offer some projection as to how effective these T cell therapies might be in the individual. While clinical trial results of HST cells are pending, we can gain some insight into the predictive value of the model by comparing the selection of escape mutations in mice with those known to occur in humans. We observed that HST cells derived from an HLA-B*5801–positive participant drove viral escape in the TW10 epitope of Gag in 14 of 14 treated mice. CTL responses to TW10 dominate during acute infection in HLA-B*57/58 individuals (Altfeld et al., 2003; Goulder et al., 1996), and mutations in the third (T242) and ninth (G248) positions confer escape from these responses (Leslie et al., 2004). The most common TW10 escape mutation observed in humans with HIV subtype B is T242N, which impacts viral fitness, as demonstrated by the rapid reversion to WT when transmitted to a non–HLA-B*57/58 individual (Leslie et al., 2004). While T242N mutations were detected in 28.6% (4/14) of treated mice, the most common escape mutation observed in our model was a glycine-to-glutamate substitution at position 248 (G248E), occurring in 92.9% (13/14) of treated mice, an early-arising mutation rarely observed in humans. The G248E mutation only modestly decreases CD8⁺ T cell recognition; yet, it has been shown to severely reduce the interaction between the inhibitory killer cell immunoglobulin-like receptor (KIR)-3DL1 and HLA-B*57, thereby rendering the virus more susceptible to elimination by

KIR3DL1-expressing NK cells (Brackenridge et al., 2011). Since our model evaluated viral escape largely in the absence of NK cells, our findings are in line with previous studies supporting a model in which a G248E mutation with limited fitness cost would thrive in the absence of NK cells, whereas a T242N mutation, characterized by greater fitness cost but superior escape from CD8⁺ T cells and NK cells would emerge in the presence of both cell types. Additionally, multiple compensatory mutations in the cyclophilin A binding loop of Gag (H219Q, I223V, M228I) can restore the replication ability of the virus (Brockman et al., 2007). We observed M228I compensatory mutations in 35.7% (5/14) of treated mice. Using our model, we demonstrate highly robust CD8⁺ T cell-mediated *in vivo* selection of escape mutations, including those commonly selected in people living with HIV. The selection of diverse escape mutations in our model clearly illustrates that this key limitation is in play, providing an opportunity to test strategies to overcome this critical limitation of T cell efficacy.

Several strategies have been proposed to overcome viral escape from CD8⁺ T cells. One approach is the application of a structure-based network analysis of amino acids across the HIV proteome that quantifies the topological importance of each residue (Gaiha et al., 2019; Louie et al., 2018). Mutation of residues with high network scores impaired HIV infectivity and viral replication, and the immunodominant responses of elite controllers preferentially targeted highly networked epitopes, in contrast to viremic progressors whose responses predominantly targeted poorly networked epitopes (Gaiha et al., 2019). Thus, this computational approach provides a mechanistic foundation for CD8⁺ T cell-mediated control and offers a means of identifying CD8⁺ T cell epitopes of topological importance, lending to improved immunogen design. A second approach is to refocus the immune response by vaccination with an engineered antigen—tHIVconsvX—a bivalent mosaic immunogen comprising only highly conserved regions of HIV Gag and Pol that has further been depleted of epitopes associated with rapid HIV progression (Ondondo et al., 2016). Recently, Patel et al. (2020) demonstrated that the same manufacturing platform used to generate HST cells for the present study could be applied to peptides spanning the tHIVconsvX antigen to generate “HST-NEETs” (HST cells with nonescaped epitope targeting). Experiments to evaluate the potential enhancing effect of HST-NEET products over HST cells in our HIV PDX mouse model are ongoing.

As the above HST/HST-NEET products illustrate, the ability to manipulate CD8⁺ T cells *in vitro* offers a high degree of flexibility to the PDX model, where antigen specificity can be

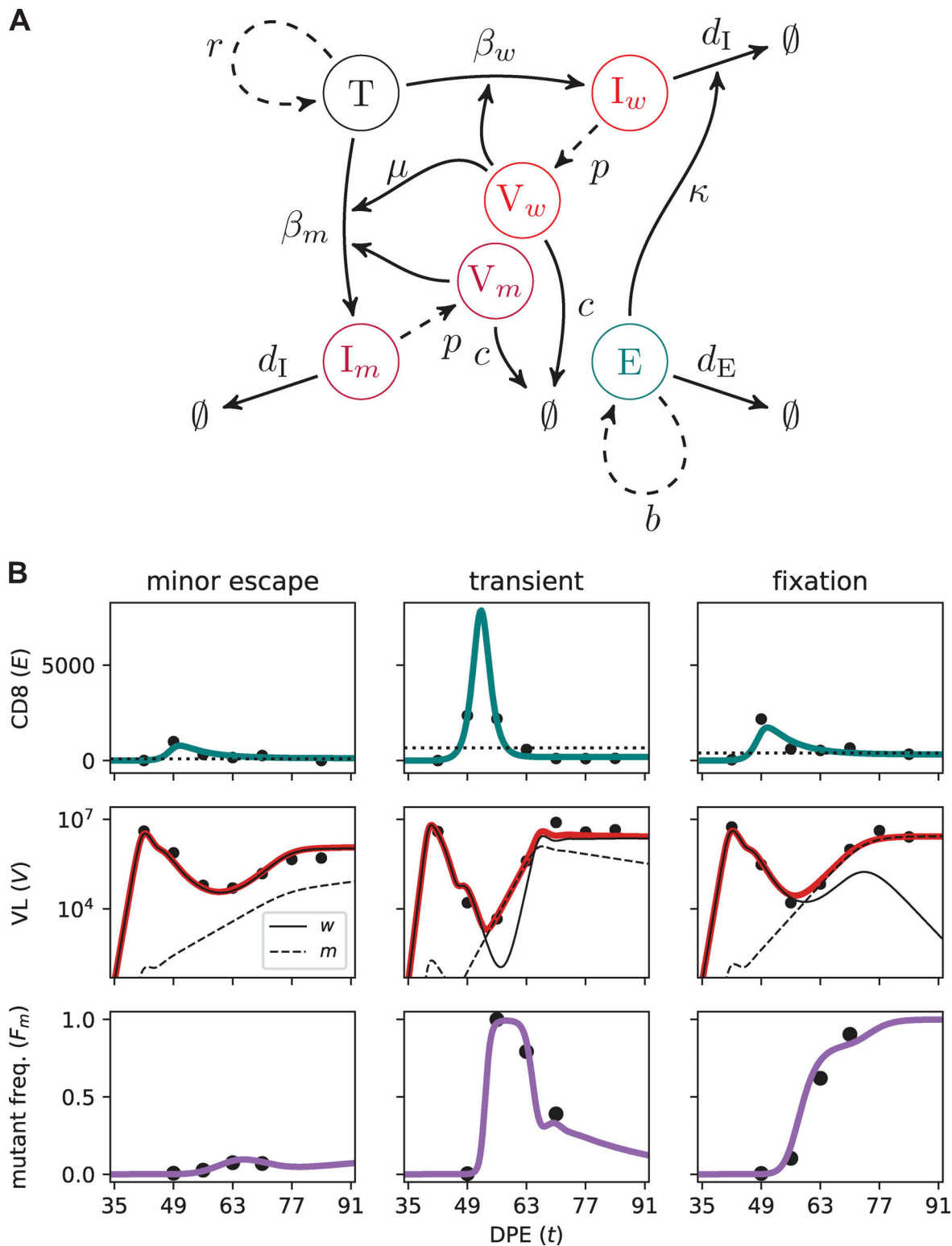


Figure 7. **Mathematical modeling reveals relationships between CD8⁺ T cells, plasma VL, and emergence of viral escape mutations across different mice.** (A) Graphical description of the mathematical model used to analyze VL, CD8⁺ T cell count, and sequencing data. Dashed arrows indicate the production of cells or virions. Solid arrows either are transitions between populations or indicate that a population has an effect on such a transition. The \emptyset symbol indicates death or clearance. The symbols placed near the arrows indicate important parameters for these processes (described in the Materials and methods) and are not necessarily identical to the transition or production rates. (B) Example fits of the viral dynamic model to data from three mice, illustrating three viral rebound scenarios (minor escape, transient, and fixation). The top panels indicate the CD8⁺ T cell concentrations and the model prediction E (teal line). The horizontal dotted line indicates the CD8⁺ T cell concentration at which the killing rate is at half maximum. The middle panels show the plasma VL data and the predicted total VL (red line). The solid and dashed black curves indicate the contributions to the VL of the WT virus (V_w) and CD8⁺ T cell escape mutant virus (V_m), respectively. The bottom panels show the measured frequency of the CD8⁺ T cell escape mutant and its predicted frequency $F_m = V_m/(V_w + V_m)$. Fits of the model to the data for all HST- and HST-NG-treated mice are shown in Fig. S4 B. DPE, days post engraftment.

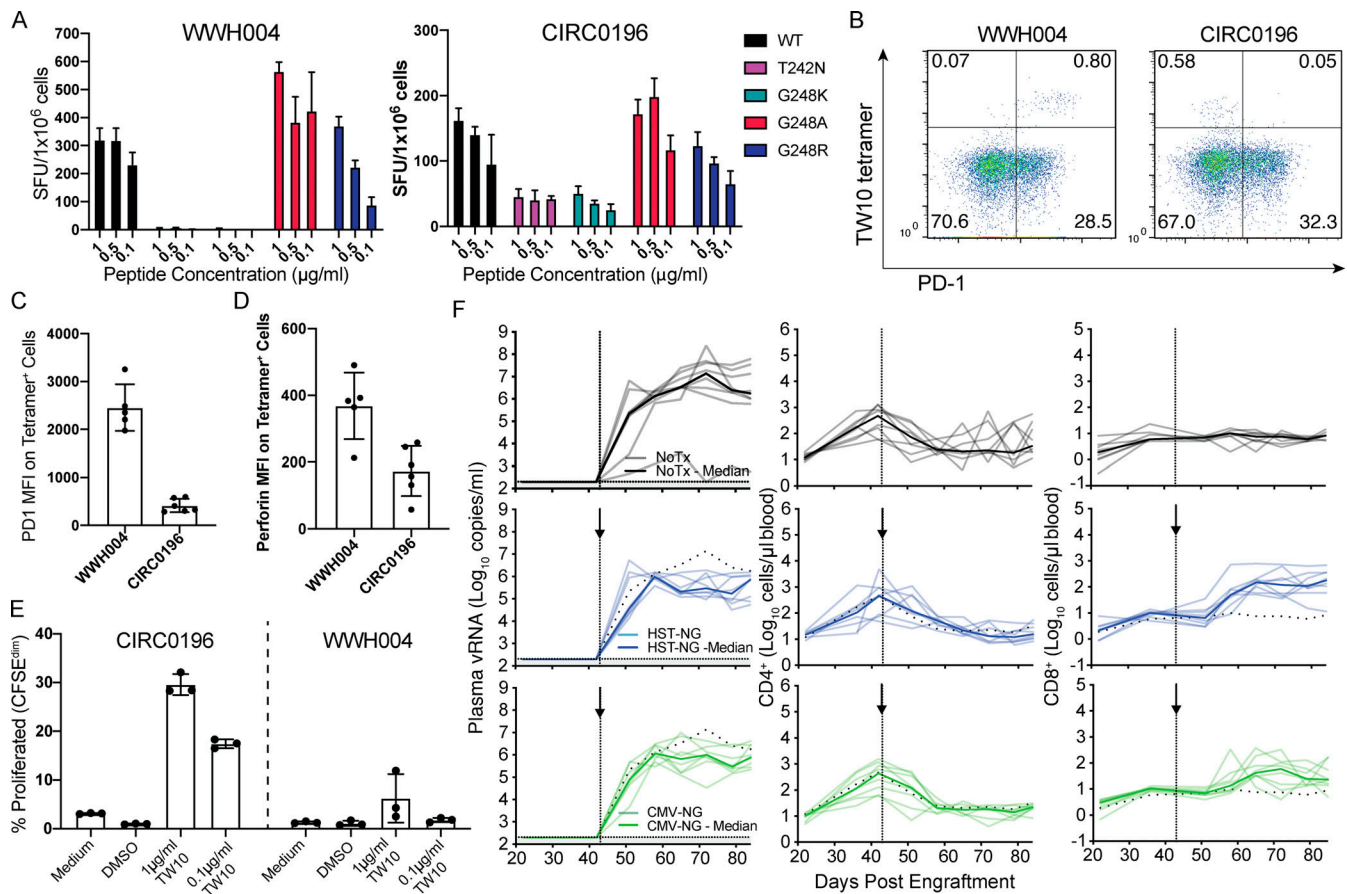


Figure 8. Marginal in vivo antiviral activity of PD-1^{hi} HST cells, despite high-magnitude response and cytotoxic phenotype. (A) Magnitudes of IFN- γ producing responses (ELISPOT) to WT TW10 epitope (WT) or a subset of the mutant epitopes selected in vivo in CIRC0196 experiments (Fig. 6). Results are shown for the HST products from CIRC0196 (used in Figs. 5, 6, and 7), as well as from a second donor (WWH004). SFU, spot-forming units. (B–D) Flow cytometry data showing that TW10-specific cells in HST cells (before infusion into mice) are PD-1^{hi} in WWH004 and PD-1^{neg} in CIRC0196 (B and C) and express higher perforin in WWH004 versus CIRC0196 (D). MFI, mean fluorescence intensity. (E) Flow cytometry-based in vitro proliferation assay results. (F) PDX results from WWH004 showing quantification of HIV plasma viral RNA (left), CD4⁺ T cells (center), and CD8⁺ T cells (right) in peripheral blood for mice that received no CD8⁺ T cells (No Tx) or IL-15SA NG-conjugated HST-NGs or CMV-specific (CMV-NG) CD8⁺ T cell products. Display and experimental details are as in Fig. 5. Error bars represent the SD.

modulated by peptide selection. In addition to allowing the evaluation of approaches to limit escape, the PDX mouse model enables the precise dissection of the roles of individual epitope-specific responses in in vivo control. For example, by omitting peptides containing the TW10 epitope from the generation of HST cells, a product devoid of this particular response could be generated, enabling precise evaluation of its overall contribution to viral control. No platform has previously been available to precisely manipulate responses to HIV and evaluate their in vivo antiviral activity.

As with any animal model, the HIV PDX mouse has limitations. One challenge is the large number of memory CD4⁺ T cells required to generate xenografts. Obtaining sufficient PBMCs from a single donor for a multicondition mouse experiment typically requires leukapheresis. Though somewhat burdensome, this procedure has nevertheless become fairly standard practice for sample collection in ART-treated donors. An additional limitation comprises deficiencies in the development of certain lymphoid structures, such as germinal centers/lymphoid follicles, which are anatomical reservoirs of HIV

replication (Bronnimann et al., 2018). Interactions between diverse human cell types not included in the model are also currently lacking, though future iterations could explore whether additional cell types can be added without reintroducing GvHD.

A key direction for further model development would be to test the degree to which it recapitulates features of HIV persistence during ART. In the current study, we demonstrated that short-term ART could suppress viral replication and enable CD4⁺ T cell recovery in PDX mice. The long experimental durations that are enabled by the lack of GvHD opens up the possibility for ART treatment for several months or more, whereas previous humanized mouse ART treatments were limited to weeks (Denton et al., 2012). This identifies the HIV PDX mouse as a promising model in which to study reservoir formation, maintenance, and rebound in the presence or absence of autologous immune effectors. The PDX model could also be applied to study therapeutic interventions against the “natural” HIV reservoirs already present in the engrafted CD4⁺ T cells. Whereas we and others have previously reported spontaneous viral rebound in

NSG mice engrafted with total CD4⁺ T cells or with PBMCs from ART-treated people with HIV (Flerin et al., 2019; Huang et al., 2018; Metcalf Pate et al., 2015), we observed a lack of autologous viral rebound within the time frames presented here (84 d). This difference is likely due to the high degree of immune activation that occurs with GvHD in total CD4⁺ T cells or PBMCs acting as a latency reversing agent. We did, however, observe rebound of autologous reservoir virus at very late time points (after day 93) in the WWH004 experiment. In future work, it will be of interest to determine whether the treatment of HIV PDX mice with latency reversing agents can reactivate reservoir viruses, thus allowing immunotherapies to be tested against bona fide reservoir-harboring cells.

Here we have described a relatively facile PDX mouse model that allows investigators to study, and to seek to overcome, key barriers to achieving T cell-mediated control of HIV replication. Importantly, this model avoids the need for human fetal tissue, which critically restricts other humanized mouse models. The ability to assess primary cells in an autologous in vivo setting has clear implications for preclinical testing and personalized therapies and provides fundamental biological insights into CD8⁺ HST cell responses and mechanisms of viral escape. We believe this model will help HIV immunologists develop therapeutics that will help reengage this arm of the immune system, alongside therapies such as bNAbs, in the pursuit of durable immunological control of HIV.

Materials and methods

Leukapheresis sample collection and processing

Study participants were recruited from the Maple Leaf Medical Clinic in Toronto, Canada, through a protocol approved by the University of Toronto Institutional Review Board or from Whitman Walker Health in Washington, D.C., through a protocol approved by the George Washington University Institution Review Board. Secondary use of these was approved by the Weill Cornell Medicine Institutional Review Board. All subjects were adults and gave written informed consent. PBMCs were isolated from leukapheresis samples via standard Ficoll gradient separation methodology and were used immediately or stored in freezing media (FBS supplemented with 10% DMSO) at -80°C . Total or memory CD4⁺ T cells were isolated from PBMCs using the EasySep Human CD4⁺ T Cell Enrichment Kit or the EasySep Human Memory CD4⁺ T Cell Enrichment Kit (STEMCELL Technologies), respectively, according to the manufacturer's recommendations, with the exception that an initial cell concentration of 10^8 cells/ml was used. Enriched CD4⁺ T cells were resuspended in RPMI 1640 supplemented with 10% FBS and 1% penicillin/streptomycin and incubated at 37°C until ready for use.

Human memory CD4⁺ T cell xenograft model

6-wk-old NSG mice (The Jackson Laboratory) were engrafted with $5\text{--}10 \times 10^6$ memory CD4⁺ T cells resuspended in 200 μl PBS via tail vein injection. Mice were bled weekly to assess human immune cell reconstitution and plasma viremia. Approximately 100 μl of peripheral blood was collected into EDTA-coated tubes via a tail vein nick technique and stored at 4°C overnight or

processed immediately. Blood was centrifuged at 3,000 rpm for 10 min to separate plasma, which was stored at -20°C before viral RNA extraction. Cell pellets were immediately stained for flow cytometric analysis according to the methods below. For experiments assessing ARV suppression, mice were administered a cocktail of ARVs (57 mg/kg TDF, 143 mg/kg FTC, and 7 mg/kg DTG) via daily s.c. injections. Mice were maintained by trained research animal technicians and received daily wellness checks under Association for Assessment and Accreditation of Laboratory Animal Care International guidelines. Procedures were performed according to protocols approved by the George Washington University Institutional Animal Care and Use Committee (protocol A242) or the Weill Cornell Medical College Institutional Animal Care and Use Committee (protocol 2018-0027).

Preparation of HIV stock and in vivo infection

Infectious viral stocks of HIV_{JR-CSF} were generated by transfecting full-length HIV_{JR-CSF} plasmid (pYK-JRCSF) into 293T cells (American Type Culture Collection; CRL-3216) using FuGENE 6 Transfection Reagent (Promega). 2 d after transfection, tissue culture media were collected, precleared by centrifugation at 2,000 rpm for 5 min, and sterile filtered through a 0.45- μm syringe filter. Virus was aliquoted and stored at -80°C . Virus was titered on TZM-bl cells as described previously (Montefiori, 2009). Mice were infected with 100,000 TCID₅₀ HIV_{JR-CSF} diluted in 100 μl total media volume via i.p. injection.

Analysis of HIV infection

HIV infection in mice was monitored weekly by measuring HIV RNA concentrations in plasma using the previously described integrase single-copy assay protocol (Cillo et al., 2014). Samples were analyzed on an ABI ViiA7 Real-Time PCR System using the following cycling parameters: 50°C for 10 min, 95°C for 10 min, followed by 40 cycles of 95°C for 15 s and 60°C for 1 min. Cycle threshold values were compared with a validated HIV RNA standard run on each plate to determine HIV RNA concentration.

Flow cytometric analysis

Flow cytometric analysis of human cells was performed using a BD LSRFortessa X-20 cytometer (BD Biosciences) and FlowJo version 10 software. The general gating strategy performed was an initial forward scatter versus side scatter (FSC/SSC) gate to exclude debris, followed by FSC area versus FSC height (FSC-A/FSC-H) to gate on singlets. A Live/Dead Aqua Fixable cell stain (Invitrogen) was used to gate on live cells. Samples were analyzed using a compensated panel of the following human-specific antibodies: BV786 anti-CD3 (clone SK7), Alexa Fluor 700 anti-CD4 (RPA-T4), BV605 anti-CD8 (RPA-T8), Alexa Fluor 488 anti-CD25 (BC96), APC-Cy7 CD69 (FN50), PE anti-HLA-DR (L243), BV421 anti-CD38 (HIT2), APC anti-CD27 (O323), PE-Cy7 anti-CD197 (CCR7; G043H7), BV650 anti-CD45RA (HI100), and PerCP-Cy5.5 anti-CD45RO (UCHL1). Fluorescent counting beads were added to each sample to determine absolute cell counts.

Proliferation assays

HST cells were thawed and labeled with 0.5 μM CFSE in PBS. Cells were plated at 100,000 cells/well in 96-well

round-bottomed plates in R10. Triplicate wells were prepared for each condition and stimulated with the indicated concentrations of TW10 peptide, with a concentration of DMSO matched to the 1 $\mu\text{g}/\text{ml}$ peptide concentration, or with no additive in R10 medium. After 48 h of incubation at 37°C and 5% CO₂, media in all wells were replaced with R10 supplemented with 20 U/ml IL-2 (National Institutes of Health, National Cancer Institute Biorepositories and Biospecimen Research Branch) and cultured for an additional 3 d. Cells were then stained with anti-CD4 BV421, anti-CD8 BV605, anti-CD3 BV786 (all antibodies from BioLegend), and Live/Dead Aqua Fixable cell stain (Invitrogen) before being run on an Attune NxT flow cytometer (Thermo Fisher Scientific) and analyzed using FlowJo software (version 10). Degrees of proliferation were assessed by gating on lymphocytes (FSC/SSC), viable cells (Aqua stain negative), CD8⁺CD4⁻, and measuring the percentage of CFSE^{dim} (gate drawn based on DMSO control).

Generation of HIV-specific and CMV-specific polyclonal T cell lines (HST cells and CMV)

HIV- and CMV-specific T cell products were generated as previously described (Patel et al., 2018; Patel et al., 2020) and were cryopreserved until the day of injection.

Phenotyping of HLA-B*5801-TW10-specific CD8⁺ T cells

HLA-B*5801-TW10 monomer was received from the National Institutes of Health Tetramer Core Facility. A 10-step tetramerization protocol of this monomer was performed as recommended by the manufacturer. Briefly, 0.32 μl Streptavidin-R-Phycoerythrin (Agilent Technologies) was added to each μg of TW10 monomer in 10 steps at 10-min intervals. HST cells were stained with tetramer-R-PE for 20 min at room temperature and costained with anti-PD-1 (CD279)-Alexa Fluor 488, clone EH12.2H7, anti-CD8-BV605 (both from BioLegend), and Live/Dead Aqua Fixable cell stain (Invitrogen). Cells were then fixed and permeabilized using the Cytofix/Cytoperm kit (BD Biosciences) following the manufacturer's instructions and then stained intracellularly with anti-perforin-PE/Cy7, clone dG9 (BD Biosciences) and anti-granzyme B-BV421, clone GB11 (BioLegend). Samples were run on an Attune NxT flow cytometer (Thermo Fisher Scientific) and analyzed using FlowJo software (version 10). Phenotypes of tetramer⁺ cells were determined after gating on viable CD8⁺ cells.

IL-15SA NG cellular loading

CD8⁺ HST cell clones or bulk ex vivo expanded CD8⁺ HST cells were augmented with IL-15SA. T cells were collected from culture and washed twice with HBSS. Cells were resuspended at a density of 10⁸ cells/ml in preformulated IL-15SA NG at various concentrations and incubated at 37°C for 1 h. IL-15SA NG was provided by Repertoire Immune Medicines and was synthesized by chemically cross-linking IL-15SA with a reversible cross-linker to allow IL-15SA release over time. IL-15SA is composed of an IgG-Fc domain fused with IL-15 receptor α sushi domains that are noncovalently bonded to IL-15. Cells were washed twice in HBSS, resuspended in complete culture media, and kept at 37°C until ready for use. Cell priming resulted in ~ 120 ng IL-15SA/5 $\times 10^6$ cells.

In vitro killing assay

CD4⁺ T cells were enriched from donor PBMCs as described above and activated for 48 h at 37°C in RPMI 1640 + 10% FBS + 1% penicillin/streptomycin media supplemented with 1 $\mu\text{g}/\text{ml}$ each of anti-CD3 (clone OKT3; BioLegend), anti-CD28 (clone CD28.2; BioLegend), and 50 U/ml IL-2. Half of the activated CD4⁺ T cells were pulsed with HIV Env RLRDLLLIVTR (RR11) peptide (GenScript) at a concentration of 1 $\mu\text{g}/\text{ml}$ for 4 h. CD4⁺ T cells were then washed twice to remove any unbound peptide. To determine killing, CD8⁺ T cell clone specificity was confirmed by CD107a degranulation assay the day before assay setup. RR11-specific CD8⁺ T cell clones were co-cultured with the activated CD4⁺ T cells with or without RR11 peptide at the indicated effector-to-target ratio for 18 h at 37°C. Cells were harvested and stained for flow cytometric analysis.

IFN- γ ELISA

Plasma cytokine levels were determined using the ELISA MAX Deluxe Set Human IFN- γ Kit (BioLegend) according to the manufacturer's recommendations. Plasma was diluted 1:1 or 1:10 in 1 \times Assay Diluent A. Optical density was read at 450 nm and 570 nm using a SpectraMax i3x platform (Molecular Devices).

Sequence analysis of plasma viral RNA

The presence of viral escape mutations was determined by sequence analysis of a 974-bp region of HIV *gag-pol*. Viral RNA was extracted from plasma using the QIAamp Viral RNA Mini Kit (Qiagen) according to the manufacturer's recommendations and eluted in 60 μl nuclease-free water. cDNA generation (Expand Reverse transcription; Roche) and subsequent nested PCR (Expand High Fidelity PCR kit; Roche) were performed using HIV-specific primers. Second-round PCR amplicons were processed with Nextera XT DNA library preparation kits (Illumina) according to the manufacturer's specifications. Dual-indexed libraries (Nextera XT index kit; Illumina) were multiplexed and sequenced using MiSeq version 2 paired-end kits (2 \times 250 bp). MiSeq reads were processed using an in-house pipeline, MiCall (Chui et al., 2015), that uses an iterative remapping algorithm to accurately detect amino acid substitutions present at $\geq 1\%$ frequency in a highly variable viral population (Lee et al., 2020).

Statistical analysis

Statistical analyses were conducted using GraphPad Prism 9, SAS version 9.4, or R version 3.6.3 software. In vitro experiments with fewer than six replicates per group were analyzed using pairwise Student's *t* test. Prior to completing in vivo mouse experiments, sample size calculations based on an independent two-sample pooled *t* test determined that a minimum of five mice per group were necessary to detect a mean 1- \log_{10} decrease in HIV RNA (VL) at a single time point for a treatment group as compared with a control group (Fig. S2). For all in vivo experiments, at least five mice were included in each treatment group. Longitudinal in vivo data (HIV RNA and CD4⁺ and CD8⁺ T cell counts) were compared between groups using linear median quantile mixed-effects models in the R lqmm package with random intercepts only; bootstrap estimates for the fitted models were then obtained using 500 replicates per model.

Treatment group comparisons were corrected for multiple comparisons using the multivariate *t*-distribution method in the R emmeans package. Two approaches were used for VL: (1) considering all time points from post-CD8⁺ T cell infusion through the end of the experiment (Tables 1 and 2) and (2) considering time points from 1 wk to 3 wk after CD8⁺ T cell infusion, after which point escape mutations were shown to appear for CIRC0196. This coincides with days 42–56 for CIRC0196 (Fig. 5) and days 49–63 for WWH004 (Fig. 8). Single time points were assessed using Brown-Forsythe and Welch one-way ANOVA with Dunnett's post hoc multiple comparisons test. Differences were considered statistically significant at $P < 0.05$. Error bars in all figures represent SD.

Generation and maintenance of CD8⁺ HST cell clones

CD8⁺ HST cell responses from study participants were mapped by IFN- γ ELISPOT, using 270 previously defined HIV optimal CD8⁺ epitopes restricted by common HLA alleles (Goulder and Walker, 2012). CD8⁺ T cell clones to the targeted peptides were established from PBMCs of HIV-infected study participants by stimulating 10^7 cells/well in a 24-well plate with 10 μ g/ml of peptide for 4 h. T cells that had produced IFN- γ in response to this stimulation were enriched using an IFN- γ secretion, detection, and enrichment kit (Miltenyi Biotec), following the manufacturer's instructions. These cells were plated at a series of dilutions in 96-well plates with feeder medium (RPMI 1640 supplemented with 10% FBS and PenStrep [RPMI-10] with 10^6 cells/ml 5,000 rad irradiated PBMCs + 50 IU/ml IL-2 + 100 ng/ml each of anti-CD3 [OKT3; eBioscience] and anti-CD28 [CD28.2; eBioscience]). 1 mo later, colonies were selected from the lowest dilution plate with positive wells (less than one in five of wells positive) and screened for responsiveness to peptide by IFN- γ ELISPOT assay. Positive clones were expanded biweekly with feeder medium (RPMI-10 media, 100 ng/ml each of anti-CD3 and anti-CD28 antibody, 10^6 irradiated PBMCs/ml). Clone specificity and activity were confirmed by degranulation assay (CD107a flow cytometry) within 1 d of setting up injection into mice.

IFN- γ ELISPOT assay

Staphylococcal enterotoxin B (SEB) was used as a positive control (Sigma-Aldrich), and either cells alone (negative control, no peptides) or actin (JPT Technologies) was used as an irrelevant antigen control. HST cells were plated at 10^5 /well on anti-IFN- γ -coated ELISPOT plates (MilliporeSigma). Positive responses were defined as having more than four times the spot-forming cells obtained in the negative control actin. For epitope mapping, peptides were mixed into pools of 10–15 peptides before T cell stimulation on an ELISPOT. Using matrices, cross-reactive pools were analyzed for common epitopes, and these peptides were then individually tested on ELISPOT to confirm specificity.

Chromium release cytotoxicity assay

The cytotoxic ability of HST cells was determined with a chromium-51 release assay. Autologous PHAb targets were pulsed with nothing (negative control) or HST PepMix and incubated with chromium-51 for 1 h. Targets were washed three times and co-cultured with autologous effector T cells at varying

effector-to-target ratios for 4 h. The chromium-51 release assay was set up as previously described (Patel et al., 2018). Specific lysis percentage was measured as: (Experimental release/spontaneous release)/(maximum release/spontaneous release) \times 100.

Multiplex assay

Polyfunctionality of HST products was assessed with a Bio-Plex Pro Human 17-plex Cytokine Assay kit (Bio-Rad Laboratories). HST cells were washed and plated at 10^6 cells/well with 1 μ l of corresponding PepMix: actin, HST, or SEB. The next day, supernatants were harvested from the wells and assessed based on Bio-Rad multiplex protocol. Samples were analyzed for concentrations of cytokines based on the standard curves produced.

Degranulation assay

Prior to use in in vivo or in vitro assays, the specificity and functionality of HIV-specific CD8⁺ T cell clones were assessed by peptide pulse and degranulation assay. Approximately 10^5 CTLs were collected from culture and transferred to a 96-well plate. 1 μ l of anti-human CD107a antibody was added and mixed thoroughly before being split into two wells. 1 ng/ μ l of appropriate peptide was added to one well (the other well served as a negative control), and cells were incubated at 37°C for 4 h. After 4 h, cells were washed and stained for surface expression of CD4 (Alexa Fluor 700 anti-CD4 [RPA-T4]) and CD8 (BV605 anti-CD8 [RPA-T8]), and Live/Dead Aqua Fixable cell stain (Invitrogen) before being run on a BD LSRFortessa I flow cytometer and analyzed using FlowJo software (version 10).

Modeling viral dynamics

To describe the VL, CD8⁺ T cell counts, and the HIV sequence data, we extended the standard viral dynamics model (Perelson, 2002; Perelson and Ribeiro, 2013) by including an effector cell population that can kill cells infected by the WT virus and a mutant virus that is resistant to the CD8⁺ T cell response (Ganusov et al., 2013; Yang and Ganusov, 2018). The model describes the changes in the concentrations of infected cells I_w (WT) and I_m (mutant), the CD8⁺ T cells E , and target cells T , i.e., CD4⁺ T cells susceptible to infection in terms of a system of ordinary differential equations (ODEs). A graphical description of the ODE model is shown in Fig. 7 A.

We assume the target cell population grows logistically with exponential growth rate r and carrying capacity K (Sachsenberg et al., 1998). We write $N = T + I_w + I_m$ for the total CD4⁺ T cell concentration. Infection of target cells is assumed to occur at a rate proportional to the product of the virus concentration and the fraction of the uninfected cells T/N , and the infection rate constant β is assumed to differ between the WT (w) and the mutant (m) virus. Infected cells produce virions at rate p per cell, and free virions are cleared at rate c per virion. As the dynamics of free virus are fast compared with the other populations, we can simplify the model by assuming that the number of (rapidly produced and cleared) virions is proportional to the number of infected cells (i.e., $V_w = I_w \cdot p/c$ and $V_m = I_m \cdot p/c$; De Boer and Perelson, 1998). With probability μ , the infection of a target cell with the WT virus results in an infected cell with an escape mutation. We ignore the smaller rate of reversion to the WT and

assume that the mice are initially infected with only the WT virus. Infected cells die due to viral cytopathic effects at rate d_i , and only cells infected with the WT virus are killed by effector cells at maximum rate κ . The rate of killing is assumed to saturate at high concentrations of effector cells, and the killing rate is at half maximum at effector cell concentration h .

Effector cells are assumed to expand independently of antigen concentration in a “programmed” manner. We use a simplification of a T cell response model developed for lymphocytic choriomeningitis virus in mice (Althaus et al., 2007; De Boer et al., 2001). Before time τ , the effector cell concentration E grows exponentially at rate b . After time τ , the effector cell concentration contracts exponentially at rate d_E (Yang and Ganusov, 2018) to the steady-state value λ_E . We use a smoothed step function $H_t = (1 + e^{\tau-t})^{-1}$ to make the transition between expansion and contraction more gradual. This leads to the following system of ODEs:

$$\begin{aligned} \frac{dT}{dt} &= rT \left(1 - \frac{N}{K}\right) - (\beta_w V_w + \beta_m V_m) \frac{T}{N} \\ \frac{dI_w}{dt} &= (1 - \mu)\beta_w V_w \frac{T}{N} - d_i I_w - \kappa \frac{I_w E}{h + E} \\ \frac{dI_m}{dt} &= (\mu\beta_w V_w + \beta_m V_m) \frac{T}{N} - d_i I_m \\ \frac{dE}{dt} &= (1 - H_t)bE - H_t d_E \cdot (E - \lambda_E) \end{aligned}$$

with initial conditions $T(t_0) = K$, $I_w(t_0) = I_0$, $I_m(t_0) = 0$, and $E(t_0) = E_0$. The initial time (t_0) is set to the time of infection (35 days post engraftment).

Parameter estimation

Despite the high level of homogeneity expected in this experiment, small differences between individual mice are to be anticipated. Moreover, escape from CTL responses by mutation is a stochastic process. Therefore, we estimated parameters in a nonlinear mixed-effects modeling framework. This also allowed us to incorporate treatment type as a covariate. The population- and individual-level parameters were estimated using Monolix (<https://lixoft.com/>). We allowed for random effects on parameters K , β_w , β_m , I_0 , κ , h , b , τ , d_E , λ_E , and E_0 . The mutation rate was assumed to be the same between mice, and the parameters $p = 2 \cdot 10^3 d^{-1}$ and $c = 23 d^{-1}$ were kept constant at previously estimated values (Haase et al., 1996; Ramratnam et al., 1999) as they are not identifiable. We assessed the identifiability of the parameters (excluding the constants p and c) with the Mathematica IdentifiabilityAnalysis package (Anguelova et al., 2012) and found that the model is locally structurally identifiable, meaning that with ideal data, we should be able to identify all parameters. Nonetheless, we found that the parameters d_i and r were difficult to identify in practice, and hence we fixed d_i to $0.6 d^{-1}$ as estimated previously (Ikeda et al., 2014; Whitney et al., 2014) and r to $3 d^{-1}$.

Using only the ODE for the effector cells (dE/dt) and the CD8⁺ T cell data, we determined which parameters were affected by the type of treatment (HST, HST-NG) by selecting the model with the smallest Akaike information criterion (AIC) value. In

the selected model, the treatment type was a covariate for the parameters τ , b , d_E , and λ_E . We assessed the statistical evidence for treatment effects on these parameters by AIC-based model comparison. Excluding the treatment effect on τ resulted in an AIC difference (ΔAIC) of 25, and excluding the effect on d_E led to $\Delta AIC = 10$. Additionally, in the full model, mice treated with CMV-specific CD8⁺ T cells tended to have a smaller carrying capacity K for the target cells, and hence CMV was added as a covariate for K .

As a measurement model, we took a log-normal distribution for the VL and estimated the SD. For the CD8⁺ T cell concentration, we argued that one would expect to find a Poisson-distributed number of CD8⁺ HST cells in a sample of a given volume, and hence the SD should be proportional (allowing for overdispersion) to \sqrt{E} . To accomplish this, we used a normal distribution with constant SD for the square root-transformed CD8⁺ T cell data. Finally, we used a logit-normal distribution to model the frequency of the escape mutant $F_m = V_m/(V_w + V_m)$. Here we had to fix the SD $\sigma_F = 0.7$ in order to avoid divergence of the likelihood.

Online supplemental material

Fig. S1 shows the results of flow cytometric analysis and the gating strategy. Fig. S2 displays the results of statistical analysis of the PDX mouse model HIV infection and power calculation. Fig. S3 provides the characterization of immune effectors used in PDX mice. Fig. S4 gives parameter estimates for individual mice grouped by treatment and fits of the ODE model for all mice treated with HST and HST-NG. Fig. S5 displays the clinical characteristics of study participants.

Acknowledgments

The authors thank the study participants and the staff at the Maple Leaf Medical Clinic. We also thank Dr. James Whitney (Boston College, Boston, MA) for providing the preformulated antiretroviral drug cocktail. The following reagents were obtained through the National Institutes of Health AIDS Reagent Program, Division of AIDS, National Institute of Allergy and Infectious Diseases, National Institutes of Health: HIV-1 JR-CSF Infectious Molecular Clone (pYK-JRCSE, catalog no. 2708) from Dr. Irvin S.Y. Chen and Dr. Yoshio Koyanagi, HIV-1 Consensus B Gag Peptide Set (catalog no. 8117), HIV-1 Consensus B Pol Peptide Set (catalog no. 6208), and HIV-1 Consensus B Nef Peptide Set (catalog no. 5189). The following reagent was obtained through the National Institutes of Health Tetramer Core Facility: HLA-B*5801-TW10 monomer.

Research reported in this publication was supported by the National Institute of Allergy and Infectious Diseases of the National Institutes of Health (R01 AI028433 and P01 AI131365 to A.S. Perelson; R33 AI122391, R21 AI152828, R01 AI47845, and UM1AI126617 to R.B. Jones), with co-funding support from the National Institute on Drug Abuse, the National Institute of Mental Health, and the National Institute of Neurological Disorders and Stroke (UM1AI126617); by the National Institutes of Health Office of the Director (R01 OD011095 to A.S. Perelson); and by the National Center for Advancing Translational Sciences

of the National Institutes of Health (TL1TR002386 to C.D. McCann). This research was also facilitated by a pilot grant from the District of Columbia Developmental Center for AIDS Research, a National Institutes of Health-funded program (AI117970) that is supported by the following National Institutes of Health co-funding and participating institutes and centers: National Institute of Allergy and Infectious Diseases; National Cancer Institute; Eunice Kennedy Shriver National Institute of Child Health and Human Development; National Heart, Lung, and Blood Institute; National Institute on Drug Abuse; National Institute of Mental Health; National Institute on Aging; Fogarty International Center; National Institute of General Medical Sciences; National Institute of Diabetes and Digestive and Kidney Diseases; and Office of AIDS Research. This research was also supported in part by grants from the Canadian Institutes of Health Research (PJT-159625 and HBI-164063 to Z.L. Brumme) and a scholar award from the Michael Smith Foundation for Health Research (to Z.L. Brumme). The content is solely the responsibility of the authors and does not necessarily represent the official views of the National Institutes of Health. Portions of this work were conducted under the auspices of the U.S. Department of Energy under contract 89233218CNA000001.

Author contributions: R.B. Jones, C.D. McCann, B.D. Walker, D.J. Irvine, and A. Danesh designed the study. C.D. McCann, C.H. van Dorp, A. Danesh, A.R. Ward, T.R. Dilling, T.M. Mota, S. Patel, C.J. Brumme, E. Zale, E.M. Stevenson, and W. Dong conducted experiments. D.S. Jones, T.L. Andresen, and C.M. Bollard provided reagents. C.D. McCann, C.H. van Dorp, and A. Danesh analyzed the data. C.H. van Dorp and A.S. Perelson developed the mathematical model. C.D. McCann and R.B. Jones wrote the manuscript. C.H. van Dorp, A. Danesh, A.R. Ward, T.R. Dilling, T.M. Mota, E. Zale, E.M. Stevenson, S. Patel, C.J. Brumme, W. Dong, D.S. Jones, T.L. Andresen, B.D. Walker, Z.L. Brumme, C.M. Bollard, A.S. Perelson, and D.J. Irvine reviewed and edited the manuscript.

Disclosures: D.S. Jones reported "other" from Repertoire Immune Medicines and "other" from Bristol Myers Squibb outside the submitted work; in addition, D.S. Jones had a patent to PCT/US2019/061837 pending and a patent to PCT/US2017/037249 pending. T.L. Andresen reported being a co-founder of Repertoire Immune Medicine. C.M. Bollard reported "other" from Mana Therapeutics outside the submitted work; in addition, C.M. Bollard had a patent number 9,885,021 licensed to Mana Therapeutics. C.M. Bollard also reported being on the board of directors of Cabaletta Bio, being a co-founder of Mana Therapeutics and Catamaran Bio, and having stock ownership in Repertoire Immune Medicines and Neximmune. D.J. Irvine reported "other" from Repertoire Immune Medicines during the conduct of the study; in addition, D.J. Irvine had a patent to Cell Surface Coupling of Nanoparticles with royalties paid for Repertoire Immune Medicine. No other disclosures were reported.

Submitted: 2 September 2020

Revised: 15 February 2021

Accepted: 12 April 2021

References

- Allen, T.M., X.G. Yu, E.T. Kalife, L.L. Reyor, M. Lichterfeld, M. John, M. Cheng, R.L. Allgaier, S. Mui, N. Frahm, et al. 2005. De novo generation of escape variant-specific CD8⁺ T-cell responses following cytotoxic T-lymphocyte escape in chronic human immunodeficiency virus type 1 infection. *J. Virol.* 79:12952–12960. <https://doi.org/10.1128/JVI.79.20.12952-12960.2005>
- Altfeld, M., M.M. Addo, E.S. Rosenberg, F.M. Hecht, P.K. Lee, M. Vogel, X.G. Yu, R. Draenert, M.N. Johnston, D. Strick, et al. 2003. Influence of HLA-B57 on clinical presentation and viral control during acute HIV-1 infection. *AIDS.* 17:2581–2591. <https://doi.org/10.1097/00002030-200312050-00005>
- Altfeld, M., E.T. Kalife, Y. Qi, H. Streeck, M. Lichterfeld, M.N. Johnston, N. Burgett, M.E. Swartz, A. Yang, G. Alter, et al. 2006. HLA alleles associated with delayed progression to AIDS contribute strongly to the initial CD8⁺ T cell response against HIV-1. *PLoS Med.* 3:e403. <https://doi.org/10.1371/journal.pmed.0030403>
- Althaus, C.L., V.V. Ganusov, and R.J. De Boer. 2007. Dynamics of CD8⁺ T cell responses during acute and chronic lymphocytic choriomeningitis virus infection. *J. Immunol.* 179:2944–2951. <https://doi.org/10.4049/jimmunol.179.5.2944>
- Anderson, B.E., J. McNiff, J. Yan, H. Doyle, M. Mamula, M.J. Shlomchik, and W.D. Shlomchik. 2003. Memory CD4⁺ T cells do not induce graft-versus-host disease. *J. Clin. Invest.* 112:101–108. <https://doi.org/10.1172/JCI17601>
- Anguelova, M., J. Karlsson, and M. Jirstrand. 2012. Minimal output sets for identifiability. *Math. Biosci.* 239:139–153. <https://doi.org/10.1016/j.mbs.2012.04.005>
- Behzadi, S., V. Serpooshan, W. Tao, M.A. Hamaly, M.Y. Alkawareek, E.C. Dreaden, D. Brown, A.M. Alkilany, O.C. Farokhzad, and M. Mahmoudi. 2017. Cellular uptake of nanoparticles: journey inside the cell. *Chem. Soc. Rev.* 46:4218–4244. <https://doi.org/10.1039/C6CS00636A>
- Betts, M.R., M.C. Nason, S.M. West, S.C. De Rosa, S.A. Migueles, J. Abraham, M.M. Lederman, J.M. Benito, P.A. Goepfert, M. Connors, et al. 2006. HIV nonprogressors preferentially maintain highly functional HIV-specific CD8⁺ T cells. *Blood.* 107:4781–4789. <https://doi.org/10.1182/blood-2005-12-4818>
- Bieniasz, P.D., and B.R. Cullen. 2000. Multiple blocks to human immunodeficiency virus type 1 replication in rodent cells. *J. Virol.* 74:9868–9877. <https://doi.org/10.1128/JVI.74.21.9868-9877.2000>
- Bolton, D.L., J.T. Minang, M.T. Trivett, K. Song, J.J. Tuscher, Y. Li, M. Piatak Jr., D. O'Connor, J.D. Lifson, M. Roederer, et al. 2010. Trafficking, persistence, and activation state of adoptively transferred allogeneic and autologous simian immunodeficiency virus-specific CD8⁺ T cell clones during acute and chronic infection of rhesus macaques. *J. Immunol.* 184:303–314. <https://doi.org/10.4049/jimmunol.0902413>
- Borducchi, E.N., J. Liu, J.P. Nkolola, A.M. Cadena, W.H. Yu, S. Fischinger, T. Broge, P. Abbink, N.B. Mercado, A. Chandrashekar, et al. 2018. Antibody and TLR7 agonist delay viral rebound in SHIV-infected monkeys. *Nature.* 563:360–364. <https://doi.org/10.1038/s41586-018-0600-6>
- Brackenridge, S., E.J. Evans, M. Toebes, N. Goonetilleke, M.K. Liu, K. di Gleria, T.N. Schumacher, S.J. Davis, A.J. McMichael, and G.M. Gillespie. 2011. An early HIV mutation within an HLA-B*57-restricted T cell epitope abrogates binding to the killer inhibitory receptor 3DL1. *J. Virol.* 85:5415–5422. <https://doi.org/10.1128/JVI.00238-11>
- Brockman, M.A., A. Schneidewind, M. Lahaie, A. Schmidt, T. Miura, I. Desouza, F. Ryvkin, C.A. Derdeyn, S. Allen, E. Hunter, et al. 2007. Escape and compensation from early HLA-B57-mediated cytotoxic T-lymphocyte pressure on human immunodeficiency virus type 1 Gag alter capsid interactions with cyclophilin A. *J. Virol.* 81:12608–12618. <https://doi.org/10.1128/JVI.01369-07>
- Brodie, S.J., D.A. Lewinsohn, B.K. Patterson, D. Jiyamapa, J. Krieger, L. Corey, P.D. Greenberg, and S.R. Riddell. 1999. In vivo migration and function of transferred HIV-1-specific cytotoxic T cells. *Nat. Med.* 5:34–41. <https://doi.org/10.1038/4716>
- Bronnimann, M.P., P.J. Skinner, and E. Connick. 2018. The B-cell follicle in HIV infection: barrier to a cure. *Front. Immunol.* 9:20. <https://doi.org/10.3389/fimmu.2018.00020>
- Browning, J., J.W. Horner, M. Pettoello-Mantovani, C. Raker, S. Yurasov, R.A. DePinho, and H. Goldstein. 1997. Mice transgenic for human CD4 and CCR5 are susceptible to HIV infection. *Proc. Natl. Acad. Sci. USA.* 94:14637–14641. <https://doi.org/10.1073/pnas.94.26.14637>
- Caskey, M., F. Klein, and M.C. Nussenzweig. 2019. Broadly neutralizing anti-HIV-1 monoclonal antibodies in the clinic. *Nat. Med.* 25:547–553. <https://doi.org/10.1038/s41591-019-0412-8>

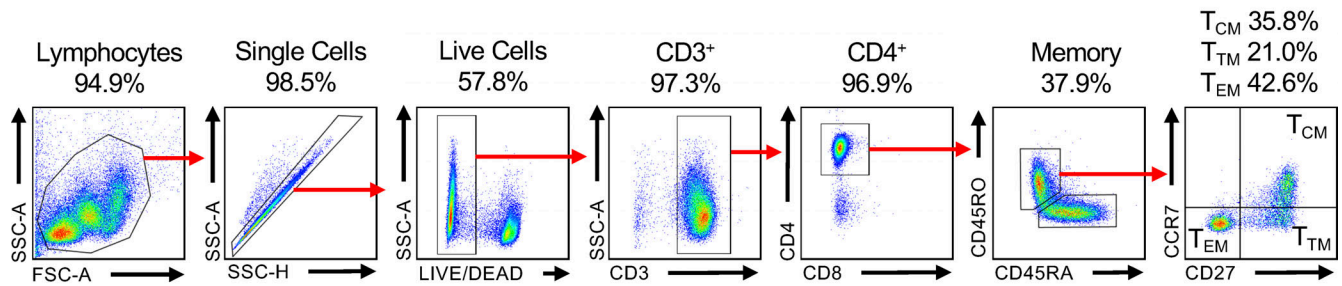
- Chen, B.J., X. Cui, G.D. Sempowski, C. Liu, and N.J. Chao. 2004. Transfer of allogeneic CD62L⁻ memory T cells without graft-versus-host disease. *Blood*. 103:1534–1541. <https://doi.org/10.1182/blood-2003-08-2987>
- Chomont, N., M. El-Far, P. Ancuta, L. Trautmann, F.A. Procopio, B. Yassine-Diab, G. Boucher, M.R. Boullassel, G. Ghattas, J.M. Brechley, et al. 2009. HIV reservoir size and persistence are driven by T cell survival and homeostatic proliferation. *Nat. Med.* 15:893–900. <https://doi.org/10.1038/nm.1972>
- Chui, C.K., W.W. Dong, J.B. Joy, A.F. Poon, W.Y. Dong, T. Mo, C.K. Woods, C. Beatty, H. Hew, P.R. Harrigan, et al. 2015. Development and validation of two screening assays for the hepatitis C virus NS3 Q80K polymorphism associated with reduced response to combination treatment regimens containing simeprevir. *J. Clin. Microbiol.* 53:2942–2950. <https://doi.org/10.1128/JCM.00650-15>
- Chun, T.W., D. Finzi, J. Margolick, K. Chadwick, D. Schwartz, and R.F. Siliciano. 1995. In vivo fate of HIV-1-infected T cells: quantitative analysis of the transition to stable latency. *Nat. Med.* 1:1284–1290. <https://doi.org/10.1038/nm1295-1284>
- Chun, T.W., L. Carruth, D. Finzi, X. Shen, J.A. DiGiuseppe, H. Taylor, M. Hermankova, K. Chadwick, J. Margolick, T.C. Quinn, et al. 1997. Quantification of latent tissue reservoirs and total body VL in HIV-1 infection. *Nature*. 387:183–188. <https://doi.org/10.1038/387183a0>
- Cillo, A.R., D. Vagratian, M.A. Bedison, E.M. Anderson, M.F. Kearney, E. Fyne, D. Koontz, J.M. Coffin, M. Piatak Jr., and J.W. Mellors. 2014. Improved single-copy assays for quantification of persistent HIV-1 viremia in patients on suppressive antiretroviral therapy. *J. Clin. Microbiol.* 52:3944–3951. <https://doi.org/10.1128/JCM.02060-14>
- Day, C.L., D.E. Kaufmann, P. Kiepiela, J.A. Brown, E.S. Moodley, S. Reddy, E.W. Mackey, J.D. Miller, A.J. Leslie, C. DePierres, et al. 2006. PD-1 expression on HIV-specific T cells is associated with T-cell exhaustion and disease progression. *Nature*. 443:350–354. <https://doi.org/10.1038/nature05115>
- Day, C.L., P. Kiepiela, A.J. Leslie, M. van der Stok, K. Nair, N. Ismail, I. Honeyborne, H. Crawford, H.M. Coovadia, P.J. Goulder, et al. 2007. Proliferative capacity of epitope-specific CD8 T-cell responses is inversely related to VL in chronic human immunodeficiency virus type 1 infection. *J. Virol.* 81:434–438. <https://doi.org/10.1128/JVI.01754-06>
- De Boer, R.J., and A.S. Perelson. 1998. Target cell limited and immune control models of HIV infection: a comparison. *J. Theor. Biol.* 190:201–214. <https://doi.org/10.1006/jtbi.1997.0548>
- De Boer, R.J., M. Oprea, R. Antia, K. Murali-Krishna, R. Ahmed, and A.S. Perelson. 2001. Recruitment times, proliferation, and apoptosis rates during the CD8⁺ T-cell response to lymphocytic choriomeningitis virus. *J. Virol.* 75:10663–10669. <https://doi.org/10.1128/JVI.75.22.10663-10669.2001>
- Denton, P.W., R. Olesen, S.K. Choudhary, N.M. Archin, A. Wahl, M.D. Swanson, M. Chateau, T. Nochi, J.F. Krisko, R.A. Spagnuolo, et al. 2012. Generation of HIV latency in humanized BLT mice. *J. Virol.* 86:630–634. <https://doi.org/10.1128/JVI.06120-11>
- Deruaz, M., and A.D. Luster. 2013. BLT humanized mice as model to study HIV vaginal transmission. *J. Infect. Dis.* 208(Suppl 2):S131–S136. <https://doi.org/10.1093/infdis/jit318>
- Dudek, T.E., D.C. No, E. Seung, V.D. Vrbancak, L. Fadda, P. Bhoumik, C.L. Boutwell, K.A. Power, A.D. Gladden, L. Battis, et al. 2012. Rapid evolution of HIV-1 to functional CD8⁺ T cell responses in humanized BLT mice. *Sci. Transl. Med.* 4:143ra98. <https://doi.org/10.1126/scitranslmed.3003984>
- Fellay, J., K.V. Shianna, D. Ge, S. Colombo, B. Ledergerber, M. Weale, K. Zhang, C. Gumbs, A. Castagna, A. Cossarizza, et al. 2007. A whole-genome association study of major determinants for host control of HIV-1. *Science*. 317:944–947. <https://doi.org/10.1126/science.1143767>
- Finzi, D., M. Hermankova, T. Pierson, L.M. Carruth, C. Buck, R.E. Chaisson, T.C. Quinn, K. Chadwick, J. Margolick, R. Brookmeyer, et al. 1997. Identification of a reservoir for HIV-1 in patients on highly active antiretroviral therapy. *Science*. 278:1295–1300. <https://doi.org/10.1126/science.278.5341.1295>
- Flerin, N.C., A. Bardhi, J.H. Zheng, M. Korom, J. Folkvord, C. Kovacs, E. Benko, R. Truong, T. Mota, E. Connick, et al. 2019. Establishment of a novel humanized mouse model to investigate *in vivo* activation and depletion of patient-derived HIV latent reservoirs. *J. Virol.* 93:e02051-18. <https://doi.org/10.1128/JVI.02051-18>
- Fontaine, P., and C. Perreault. 1990. Diagnosis of graft-versus-host disease in mice transplanted across minor histocompatibility barriers. *Transplantation*. 49:1177–1178. <https://doi.org/10.1097/O0007890-199006000-00032>
- Gaiha, G.D., E.J. Rossin, J. Urbach, C. Landeros, D.R. Collins, C. Nwonu, I. Muzhingi, M.N. Anahtar, O.M. Waring, A. Piechocka-Trocha, et al. 2019. Structural topology defines protective CD8⁺ T cell epitopes in the HIV proteome. *Science*. 364:480–484. <https://doi.org/10.1126/science.aav5095>
- Ganusov, V.V., R.A. Neher, and A.S. Perelson. 2013. Mathematical modeling of escape of HIV from cytotoxic T lymphocyte responses. *J. Stat. Mech.* 2013:P01010. <https://doi.org/10.1088/1742-5468/2013/01/P01010>
- Goulder, P.J., and B.D. Walker. 2012. HIV and HLA class I: an evolving relationship. *Immunity*. 37:426–440. <https://doi.org/10.1016/j.immuni.2012.09.005>
- Goulder, P.J., M. Bunce, P. Krausa, K. McIntyre, S. Crowley, B. Morgan, A. Edwards, P. Giangrande, R.E. Phillips, and A.J. McMichael. 1996. Novel, cross-restricted, conserved, and immunodominant cytotoxic T lymphocyte epitopes in slow progressors in HIV type 1 infection. *AIDS Res. Hum. Retroviruses*. 12:1691–1698. <https://doi.org/10.1089/aid.1996.12.1691>
- Greenblatt, M.B., V. Vrbancak, T. Tivey, K. Tsang, A.M. Tager, and A.O. Aliprantis. 2012. Graft versus host disease in the bone marrow, liver and thymus humanized mouse model. *PLoS One*. 7:e44664. <https://doi.org/10.1371/journal.pone.0044664>
- Haase, A.T., K. Henry, M. Zupancic, G. Sedgewick, R.A. Faust, H. Melroe, W. Cavert, K. Gebhard, K. Staskus, Z.Q. Zhang, et al. 1996. Quantitative image analysis of HIV-1 infection in lymphoid tissue. *Science*. 274:985–989. <https://doi.org/10.1126/science.274.5289.985>
- Halper-Stromberg, A., C.L. Lu, F. Klein, J.A. Horwitz, S. Bournazos, L. Nogueira, T.R. Eisenreich, C. Liu, A. Gazumyan, U. Schaefer, et al. 2014. Broadly neutralizing antibodies and viral inducers decrease rebound from HIV-1 latent reservoirs in humanized mice. *Cell*. 158:989–999. <https://doi.org/10.1016/j.cell.2014.07.043>
- Horton, H., I. Frank, R. Baydo, E. Jalbert, J. Penn, S. Wilson, J.P. McNevin, M.D. McSweyn, D. Lee, Y. Huang, et al. 2006. Preservation of T cell proliferation restricted by protective HLA alleles is critical for immune control of HIV-1 infection. *J. Immunol.* 177:7406–7415. <https://doi.org/10.4049/jimmunol.177.10.7406>
- Huang, W., and N.J. Chao. 2017. Memory T cells: a helpful guard for allogeneic hematopoietic stem cell transplantation without causing graft-versus-host disease. *Hematol. Oncol. Stem Cell Ther.* 10:211–219. <https://doi.org/10.1016/j.hemonc.2017.05.006>
- Huang, S.H., Y. Ren, A.S. Thomas, D. Chan, S. Mueller, A.R. Ward, S. Patel, C.M. Bollard, C.R. Cruz, S. Karandish, et al. 2018. Latent HIV reservoirs exhibit inherent resistance to elimination by CD8⁺ T cells. *J. Clin. Invest.* 128:876–889. <https://doi.org/10.1172/JCI97555>
- Ikeda, H., R.J. de Boer, K. Sato, S. Morita, N. Misawa, Y. Koyanagi, K. Aihara, and S. Iwami. 2014. Improving the estimation of the death rate of infected cells from time course data during the acute phase of virus infections: application to acute HIV-1 infection in a humanized mouse model. *Theor. Biol. Med. Model.* 11:22. <https://doi.org/10.1186/1742-4682-11-22>
- Jespersen, H., M.F. Lindberg, M. Donia, E.M.V. Söderberg, R. Andersen, U. Keller, L. Ny, I.M. Svane, L.M. Nilsson, and J.A. Nilsson. 2017. Clinical responses to adoptive T-cell transfer can be modeled in an autologous immune-humanized mouse model. *Nat. Commun.* 8:707. <https://doi.org/10.1038/s41467-017-00786-z>
- Jones, R.B., and B.D. Walker. 2016. HIV-specific CD8⁺ T cells and HIV eradication. *J. Clin. Invest.* 126:455–463. <https://doi.org/10.1172/JCI80566>
- Jones, R.B., L.C. Ndhlovu, J.D. Barbour, P.M. Sheth, A.R. Jha, B.R. Long, J.C. Wong, M. Satkunarajah, M. Schweneker, J.M. Chapman, et al. 2008. Tim-3 expression defines a novel population of dysfunctional T cells with highly elevated frequencies in progressive HIV-1 infection. *J. Exp. Med.* 205:2763–2779. <https://doi.org/10.1084/jem.20081398>
- Jones, R.B., K.E. Garrison, S. Mujib, V. Mihajlovic, N. Aidarus, D.V. Hunter, E. Martin, V.M. John, W. Zhan, N.F. Faruk, et al. 2012. HERV-K-specific T cells eliminate diverse HIV-1/2 and SIV primary isolates. *J. Clin. Invest.* 122:4473–4489. <https://doi.org/10.1172/JCI64560>
- Jones, R.B., S. Mueller, R. O'Connor, K. Rimpel, D.D. Sloan, D. Karel, H.C. Wong, E.K. Jeng, A.S. Thomas, J.B. Whitney, et al. 2016. A subset of latency-reversing agents expose HIV-infected resting CD4⁺ T-cells to recognition by cytotoxic T-lymphocytes. *PLoS Pathog.* 12:e1005545. <https://doi.org/10.1371/journal.ppat.1005545>
- Jones, R.B., S. Mueller, S. Kumari, V. Vrbancak, S. Genel, A.M. Tager, T.M. Allen, B.D. Walker, and D.J. Irvine. 2017. Antigen recognition-triggered drug delivery mediated by nanocapsule-functionalized cytotoxic T-cells. *Biomaterials*. 117:44–53. <https://doi.org/10.1016/j.biomaterials.2016.11.048>

- Julg, B., P.T. Liu, K. Wagh, W.M. Fischer, P. Abbink, N.B. Mercado, J.B. Whitney, J.P. Nkolola, K. McMahan, L.J. Tartaglia, et al. 2017. Protection against a mixed SHIV challenge by a broadly neutralizing antibody cocktail. *Sci. Transl. Med.* 9:eaa04235. <https://doi.org/10.1126/scitranslmed.aao4235>
- June, C.H., and M. Sadelain. 2018. Chimeric antigen receptor therapy. *N. Engl. J. Med.* 379:64–73. <https://doi.org/10.1056/NEJMra1706169>
- Kiepiela, P., A.J. Leslie, I. Honeyborne, D. Ramduth, C. Thobakgale, S. Chetty, P. Rathnavalu, C. Moore, K.J. Pfafferoth, L. Hilton, et al. 2004. Dominant influence of HLA-B in mediating the potential co-evolution of HIV and HLA. *Nature*. 432:769–775. <https://doi.org/10.1038/nature03113>
- Kiepiela, P., K. Ngumbela, C. Thobakgale, D. Ramduth, I. Honeyborne, E. Moodley, S. Reddy, C. de Pierres, Z. Mncube, N. Mkhwanazi, et al. 2007. CD8⁺ T-cell responses to different HIV proteins have discordant associations with VL. *Nat. Med.* 13:46–53. <https://doi.org/10.1038/nm1520>
- Kleiner, G., A. Marcuzzi, V. Zanin, L. Monasta, and G. Zauli. 2013. Cytokine levels in the serum of healthy subjects. *Mediators Inflamm.* 2013:434010. <https://doi.org/10.1155/2013/434010>
- Koenig, S., A.J. Conley, Y.A. Brewah, G.M. Jones, S. Leath, L.J. Boots, V. Davey, G. Pantaleo, J.F. Demarest, C. Carter, et al. 1995. Transfer of HIV-1-specific cytotoxic T lymphocytes to an AIDS patient leads to selection for mutant HIV variants and subsequent disease progression. *Nat. Med.* 1:330–336. <https://doi.org/10.1038/nm0495-330>
- Lam, S., J. Sung, C. Cruz, P. Castillo-Caro, M. Ngo, C. Garrido, J. Kuruc, N. Archin, C. Rooney, D. Margolis, et al. 2015. Broadly-specific cytotoxic T cells targeting multiple HIV antigens are expanded from HIV+ patients: implications for immunotherapy. *Mol. Ther.* 23:387–395. <https://doi.org/10.1038/mt.2014.207>
- Lee, E.R., N. Parkin, C. Jennings, C.J. Brumme, E. Enns, M. Casadella, M. Howison, M. Coetzer, S. Avila-Rios, R. Capina, et al. 2020. Performance comparison of next generation sequencing analysis pipelines for HIV-1 drug resistance testing. *Sci. Rep.* 10:1634. <https://doi.org/10.1038/s41598-020-58544-z>
- Leen, A.M., G.D. Myers, U. Sili, M.H. Huls, H. Weiss, K.S. Leung, G. Carrum, R.A. Krance, C.C. Chang, J.J. Mollndrem, et al. 2006. Monoculture-derived T lymphocytes specific for multiple viruses expand and produce clinically relevant effects in immunocompromised individuals. *Nat. Med.* 12:1160–1166. <https://doi.org/10.1038/nm1475>
- Leslie, A.J., K.J. Pfafferoth, P. Chetty, R. Draenert, M.M. Addo, M. Feeney, Y. Tang, E.C. Holmes, T. Allen, J.G. Prado, et al. 2004. HIV evolution: CTL escape mutation and reversion after transmission. *Nat. Med.* 10:282–289. <https://doi.org/10.1038/nm992>
- Lieberman, J., P.R. Skolnik, G.R. Parkerson III, J.A. Fabry, B. Landry, J. Bethel, and J. Kagan. 1997. Safety of autologous, ex vivo-expanded human immunodeficiency virus (HIV)-specific cytotoxic T-lymphocyte infusion in HIV-infected patients. *Blood*. 90:2196–2206. <https://doi.org/10.1182/blood.V90.6.2196>
- Liu, B., M. Jones, L. Kong, T. Noel, E.K. Jeng, S. Shi, C.G. England, S. Alter, J.S. Miller, W. Cai, et al. 2018. Evaluation of the biological activities of the IL-15 superagonist complex, ALT-803, following intravenous versus subcutaneous administration in murine models. *Cytokine*. 107:105–112. <https://doi.org/10.1016/j.cyto.2017.12.003>
- Louie, R.H.Y., K.J. Kaczorowski, J.P. Barton, A.K. Chakraborty, and M.R. McKay. 2018. Fitness landscape of the human immunodeficiency virus envelope protein that is targeted by antibodies. *Proc. Natl. Acad. Sci. USA*. 115:E564–E573. <https://doi.org/10.1073/pnas.1717765115>
- Marsden, M.D., and J.A. Zack. 2015. Studies of retroviral infection in humanized mice. *Virology*. 479–480:297–309. <https://doi.org/10.1016/j.virol.2015.01.017>
- McMichael, A.J., P. Borrow, G.D. Tomaras, N. Goonetilleke, and B.F. Haynes. 2010. The immune response during acute HIV-1 infection: clues for vaccine development. *Nat. Rev. Immunol.* 10:11–23. <https://doi.org/10.1038/nri2674>
- Melkus, M.W., J.D. Estes, A. Padgett-Thomas, J. Gatlin, P.W. Denton, F.A. Othieno, A.K. Wege, A.T. Haase, and J.V. Garcia. 2006. Humanized mice mount specific adaptive and innate immune responses to EBV and TSST-1. *Nat. Med.* 12:1316–1322. <https://doi.org/10.1038/nm1431>
- Metcalfe Pate, K.A., C.W. Pohlmeier, V.E. Walker-Sperling, J.B. Foote, K.M. Najjarro, C.G. Cryer, M. Salgado, L. Gama, E.L. Engle, E.N. Shirk, et al. 2015. A murine viral outgrowth assay to detect residual HIV type 1 in patients with undetectable VLs. *J. Infect. Dis.* 212:1387–1396. <https://doi.org/10.1093/infdis/jiv230>
- Migueles, S.A., M.S. Sabbaghian, W.L. Shupert, M.P. Bettinotti, F.M. Marincola, L. Martino, C.W. Hallahan, S.M. Selig, D. Schwartz, J. Sullivan, et al. 2000. HLA B*5701 is highly associated with restriction of virus replication in a subgroup of HIV-infected long term nonprogressors. *Proc. Natl. Acad. Sci. USA*. 97:2709–2714. <https://doi.org/10.1073/pnas.050567397>
- Migueles, S.A., A.C. Laborico, W.L. Shupert, M.S. Sabbaghian, R. Rabin, C.W. Hallahan, D. Van Baarle, S. Kostense, F. Miedema, M. McLaughlin, et al. 2002. HIV-specific CD8⁺ T cell proliferation is coupled to perforin expression and is maintained in nonprogressors. *Nat. Immunol.* 3:1061–1068. <https://doi.org/10.1038/nri845>
- Minang, J.T., M.T. Trivett, D.L. Bolton, C.M. Trubey, J.D. Estes, Y. Li, J. Smedley, R. Pung, M. Rosati, R. Jalah, et al. 2010. Distribution, persistence, and efficacy of adoptively transferred central and effector memory-derived autologous simian immunodeficiency virus-specific CD8⁺ T cell clones in rhesus macaques during acute infection. *J. Immunol.* 184:315–326. <https://doi.org/10.4049/jimmunol.0902410>
- Miura, T., M.A. Brockman, A. Schneidewind, M. Lobritz, F. Pereyra, A. Rathod, B.L. Block, Z.L. Brumme, C.J. Brumme, B. Baker, et al. 2009. HLA-B57/B*5801 human immunodeficiency virus type 1 elite controllers select for rare gag variants associated with reduced viral replication capacity and strong cytotoxic T-lymphocyte [corrected] recognition. *J. Virol.* 83:2743–2755. <https://doi.org/10.1128/JVI.02265-08>
- Montefiori, D.C. 2009. Measuring HIV neutralization in a luciferase reporter gene assay. *Methods Mol. Biol.* 485:395–405. https://doi.org/10.1007/978-1-59745-170-3_26
- Mosier, D.E., R.J. Gulizia, S.M. Baird, and D.B. Wilson. 1988. Transfer of a functional human immune system to mice with severe combined immunodeficiency. *Nature*. 335:256–259. <https://doi.org/10.1038/335256a0>
- Mota, T.M., C.D. McCann, A. Danesh, S.-H. Huang, D.B. Magat, Y. Ren, L. Leyre, T.D. Bui, T.M. Rohwetter, C.M. Kovacs, et al. 2020. Integrated assessment of viral transcription, antigen presentation, and CD8⁺ T cell function reveals multiple limitations of class I-selective histone deacetylase inhibitors during HIV-1 latency reversal. *J. Virol.* 94:e01845-19. <https://doi.org/10.1128/JVI.01845-19>
- Nishimura, Y., R. Gautam, T.W. Chun, R. Sadjadpour, K.E. Foulds, M. Shingai, F. Klein, A. Gazumyan, J. Golijanin, M. Donaldson, et al. 2017. Early antibody therapy can induce long-lasting immunity to SHIV. *Nature*. 543:559–563. <https://doi.org/10.1038/nature21435>
- Ondondo, B., H. Murakoshi, G. Clutton, S. Abdul-Jawad, E.G. Wee, H. Gatanaga, S. Oka, A.J. McMichael, M. Takiguchi, B. Korber, et al. 2016. Novel conserved-region T-cell mosaic vaccine with high global HIV-1 coverage is recognized by protective responses in untreated infection. *Mol. Ther.* 24:832–842. <https://doi.org/10.1038/mt.2016.3>
- Patel, S., R.B. Jones, D.F. Nixon, and C.M. Bollard. 2016. T-cell therapies for HIV: preclinical successes and current clinical strategies. *Cytotherapy*. 18:931–942. <https://doi.org/10.1016/j.jcyt.2016.04.007>
- Patel, S., E. Chorvinsky, S. Albiyani, C.R. Cruz, R.B. Jones, E.J. Shpall, D.M. Margolis, R.F. Ambinder, and C.M. Bollard. 2018. HIV-specific T cells generated from naive T cells suppress HIV in vitro and recognize wide epitope breadths. *Mol. Ther.* 26:1435–1446. <https://doi.org/10.1016/j.ymthe.2018.04.009>
- Patel, S., R. Hanajiri, M. Grant, D. Saunders, S. Van Pelt, M. Keller, P.J. Hanley, G. Simon, D.F. Nixon, D. Hardy, et al. 2020. HIV-specific T cells can be generated against non-escaped T cell epitopes with a GMP-compliant manufacturing platform. *Mol. Ther. Methods Clin. Dev.* 16:11–20. <https://doi.org/10.1016/j.omtm.2019.10.001>
- Perelson, A.S. 2002. Modelling viral and immune system dynamics. *Nat. Rev. Immunol.* 2:28–36. <https://doi.org/10.1038/nri700>
- Perelson, A.S., and R.M. Ribeiro. 2013. Modeling the within-host dynamics of HIV infection. *BMC Biol.* 11:96. <https://doi.org/10.1186/1741-7007-11-96>
- Pereyra, F., D. Heckerman, J.M. Carlson, C. Kadie, D.Z. Soghoian, D. Karel, A. Goldenthal, O.B. Davis, C.E. DeZiel, T. Lin, et al. 2014. HIV control is mediated in part by CD8⁺ T-cell targeting of specific epitopes. *J. Virol.* 88:12937–12948. <https://doi.org/10.1128/JVI.01004-14>
- Petrovas, C., J.P. Casazza, J.M. Brenchley, D.A. Price, E. Gostick, W.C. Adams, M.L. Precopio, T. Schacker, M. Roederer, D.C. Douek, et al. 2006. PD-1 is a regulator of virus-specific CD8⁺ T cell survival in HIV infection. *J. Exp. Med.* 203:2281–2292. <https://doi.org/10.1084/jem.20061496>
- Ramratnam, B., S. Bonhoeffer, J. Binley, A. Hurley, L. Zhang, J.E. Mittler, M. Markowitz, J.P. Moore, A.S. Perelson, and D.D. Ho. 1999. Rapid production and clearance of HIV-1 and hepatitis C virus assessed by large volume plasma apheresis. *Lancet*. 354:1782–1785. [https://doi.org/10.1016/S0140-6736\(99\)02035-8](https://doi.org/10.1016/S0140-6736(99)02035-8)
- Ren, Y., S.H. Huang, S. Patel, W.D.C. Alberto, D. Magat, D. Ahimovic, A.B. Macedo, R. Durga, D. Chan, E. Zale, et al. 2020. BCL-2 antagonism sensitizes cytotoxic T cell-resistant HIV reservoirs to elimination ex vivo. *J. Clin. Invest.* 130:2542–2559. <https://doi.org/10.1172/JCI132374>

- Rhode, P.R., J.O. Egan, W. Xu, H. Hong, G.M. Webb, X. Chen, B. Liu, X. Zhu, J. Wen, L. You, et al. 2016. Comparison of the superagonist complex, ALT-803, to IL15 as cancer immunotherapeutics in animal models. *Cancer Immunol. Res.* 4:49–60. <https://doi.org/10.1158/2326-6066.CIR-15-0093-T>
- Sachsenberg, N., A.S. Perelson, S. Yerly, G.A. Schockmel, D. Leduc, B. Hirschel, and L. Perrin. 1998. Turnover of CD4⁺ and CD8⁺ T lymphocytes in HIV-1 infection as measured by Ki-67 antigen. *J. Exp. Med.* 187:1295–1303. <https://doi.org/10.1084/jem.187.8.1295>
- Saglio, F., P.J. Hanley, and C.M. Bollard. 2014. The time is now: moving toward virus-specific T cells after allogeneic hematopoietic stem cell transplantation as the standard of care. *Cytotherapy.* 16:149–159. <https://doi.org/10.1016/j.jcyt.2013.11.010>
- Spranger, S., B. Frankenberger, and D.J. Schendel. 2012. NOD/scid IL-2Rg^{null} mice: a preclinical model system to evaluate human dendritic cell-based vaccine strategies in vivo. *J. Transl. Med.* 10:30. <https://doi.org/10.1186/1479-5876-10-30>
- Tang, L., Y. Zheng, M.B. Melo, L. Mabardi, A.P. Castaño, Y.Q. Xie, N. Li, S.B. Kudchodkar, H.C. Wong, E.K. Jeng, et al. 2018. Enhancing T cell therapy through TCR-signaling-responsive nanoparticle drug delivery. *Nat. Biotechnol.* 36:707–716. <https://doi.org/10.1038/nbt.4181>
- Trautmann, L., L. Janbazian, N. Chomont, E.A. Said, S. Gimmig, B. Bessette, M.R. Boulassel, E. Delwart, H. Sepulveda, R.S. Balderas, et al. 2006. Upregulation of PD-1 expression on HIV-specific CD8⁺ T cells leads to reversible immune dysfunction. *Nat. Med.* 12:1198–1202. <https://doi.org/10.1038/nm1482>
- Turk, G., Y. Ghiglion, J. Falivene, M.E. Socias, N. Laufer, R.S. Coloccini, A.M. Rodriguez, M.J. Ruiz, M.A. Pando, L.D. Giavedoni, et al. 2013. Early Gag immunodominance of the HIV-specific T-cell response during acute/early infection is associated with higher CD8⁺ T-cell antiviral activity and correlates with preservation of the CD4⁺ T-cell compartment. *J. Virol.* 87:7445–7462. <https://doi.org/10.1128/JVI.00865-13>
- Turnbull, E.L., A.R. Lopes, N.A. Jones, D. Cornforth, P. Newton, D. Aldam, P. Pellegrino, J. Turner, I. Williams, C.M. Wilson, et al. 2006. HIV-1 epitope-specific CD8⁺ T cell responses strongly associated with delayed disease progression cross-recognize epitope variants efficiently. *J. Immunol.* 176:6130–6146. <https://doi.org/10.4049/jimmunol.176.10.6130>
- Walker, B.D. 2007. Elite control of HIV infection: implications for vaccines and treatment. *Top. HIV Med.* 15:134–136.
- Wang, H., G. Kaur, A.I. Sankin, F. Chen, F. Guan, and X. Zang. 2019. Immune checkpoint blockade and CAR-T cell therapy in hematologic malignancies. *J. Hematol. Oncol.* 12:59. <https://doi.org/10.1186/s13045-019-0746-1>
- Wege, A.K., M.W. Melkus, P.W. Denton, J.D. Estes, and J.V. Garcia. 2008. Functional and phenotypic characterization of the humanized BLT mouse model. *Curr. Top. Microbiol. Immunol.* 324:149–165. https://doi.org/10.1007/978-3-540-75647-7_10
- Wei, S.C., C.R. Duffy, and J.P. Allison. 2018. Fundamental mechanisms of immune checkpoint blockade therapy. *Cancer Discov.* 8:1069–1086. <https://doi.org/10.1158/2159-8290.CD-18-0367>
- Whitney, J.B., and R.B. Jones. 2018. In vitro and in vivo models of HIV latency. *Adv. Exp. Med. Biol.* 1075:241–263. https://doi.org/10.1007/978-981-13-0484-2_10
- Whitney, J.B., A.L. Hill, S. Sanisetty, P. Penaloza-MacMaster, J. Liu, M. Shetty, L. Parenteau, C. Cabral, J. Shields, S. Blackmore, et al. 2014. Rapid seeding of the viral reservoir prior to SIV viraemia in rhesus monkeys. *Nature.* 512:74–77. <https://doi.org/10.1038/nature13594>
- Whitney, J.B., S.Y. Lim, C.E. Osuna, J.L. Kublin, E. Chen, G. Yoon, P.T. Liu, P. Abbink, E.N. Borducci, A. Hill, et al. 2018. Prevention of SIVmac251 reservoir seeding in rhesus monkeys by early antiretroviral therapy. *Nat. Commun.* 9:5429. <https://doi.org/10.1038/s41467-018-07881-9>
- Yang, Y., and V.V. Ganusov. 2018. Kinetics of HIV-specific CTL responses plays a minimal role in determining HIV escape dynamics. *Front. Immunol.* 9:140. <https://doi.org/10.3389/fimmu.2018.00140>

Supplemental material

Total CD4⁺ Enrichment



Memory CD4⁺ Enrichment

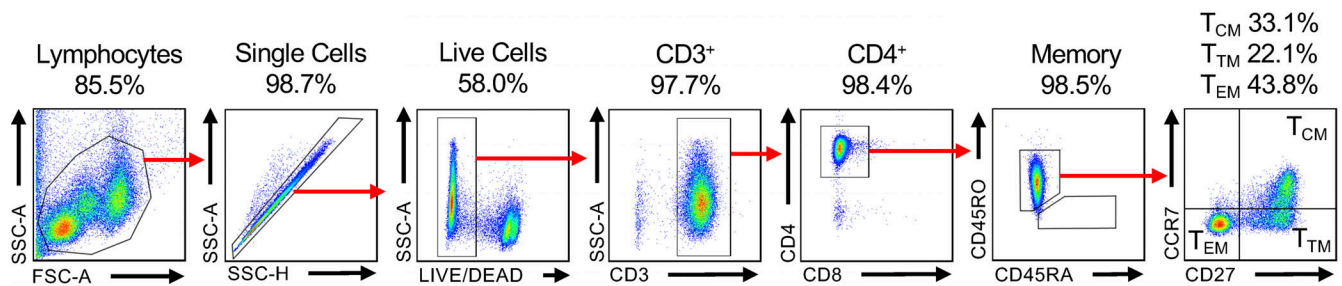


Figure S1. Flow cytometric analysis and gating strategy. Total (top) or memory (bottom) CD4⁺ T cells were enriched from donor PBMCs. Representative flow plots reveal cell population characteristics before engraftment in mice. Lymphocytes were gated based upon FSC-A and SSC-A followed by exclusion of doublets (FSC-A by FSC-H). Live cells were gated based on exclusion of amine-reactive viability dye (Live/Dead). T cells were then identified by CD3 staining and separated based on CD4⁺ versus CD8⁺ staining. Naive (CD45RA⁻/CD45RO⁻) versus memory (CD45RA⁺/CD45RO⁺) CD4⁺ T cells were identified, and memory CD4⁺ T cells were further phenotyped into T_{CM}, T_{TM}, and T_{EM} subsets based upon CCR7 and CD27 surface staining. A similar gating strategy was used to identify cellular populations from all in vivo mouse blood and tissue samples. T_{CM}, central memory T cell; T_{TM}, transitional memory T cell; T_{EM}, effector memory T cell. The results shown are representative of at least 10 independent experiments.

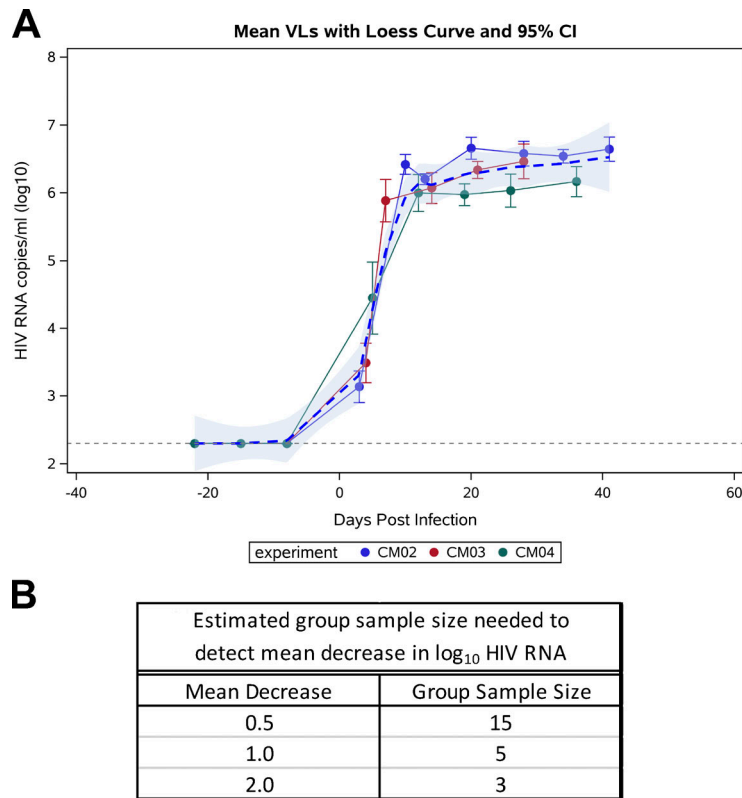


Figure S2. **Statistical analysis of PDX mouse model HIV infection and power calculation. (A)** Graph depicts locally estimated scatterplot smoothing (Loess) curve analysis with 95% confidence interval (CI; light blue shaded region) of combined data from the No Tx groups from three independent experiments. **(B)** Sample sizes were calculated using SAS Studio. Sample size calculations assume an independent two-sample pooled *t* test, one-sided test with a null difference of 0, equal group sizes, $\alpha = 0.05$, and desired power = 0.80. The control group mean and SD were estimated by pooling together the set point \log_{10} -transformed HIV RNA plasma VLs from three independent experiments, thus accounting for interexperiment variation.

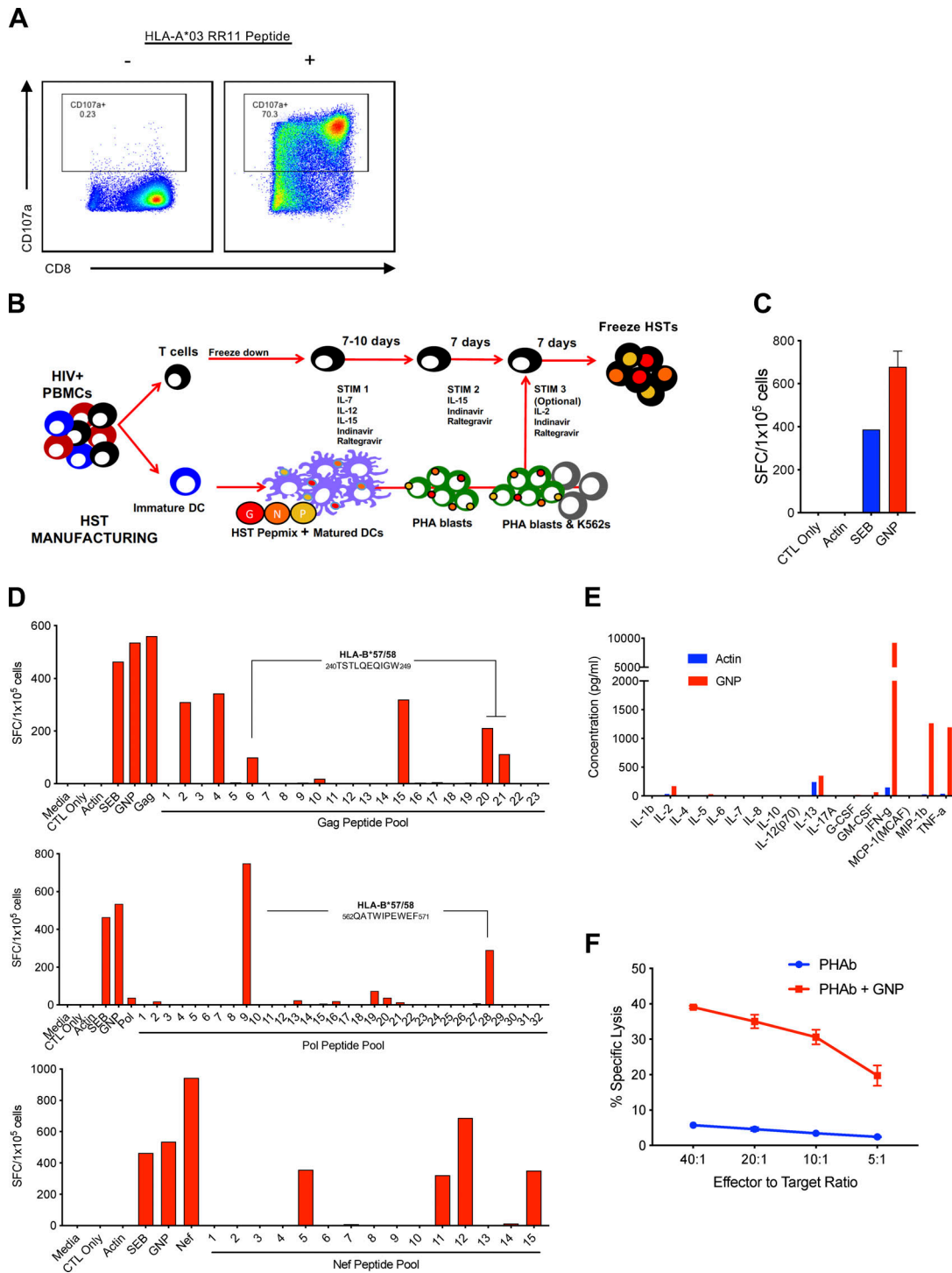


Figure S3. **Characterization of immune effectors used in PDX mice.** (A) RR11-specific CD8⁺ T cell clone was analyzed by flow cytometry for peptide specificity. Cloned CD8⁺ T cells were pulsed with 1 μg/ml RR11 peptide for 4 h in the presence of anti-CD107a (PE) antibody. After 4-h incubation, cells were washed and stained for surface expression of CD8 (BV605). Gated population displays the percentage of cells degranulating in response to cognate peptide. The results shown are representative of at least 30 independent experiments with this clone. (B–F) Generation and functional validation of HST cells. HST cells were generated from an HIV-positive study participant, CIRC0196. (B) Schematic representation of the HST manufacturing process. Cells underwent three rounds of stimulation with autologous dendritic cells (DCs) pulsed with a Gag, Nef, and Pol peptide mix (GNP pepmix). Cells were maintained in the presence of ARVs to prevent new HIV infections. (C) Functional analysis of generated HST cells was assessed by IFN-γ release in response to GNP pepmix, SEB (positive control), actin (negative control), or CTL alone (negative control), as measured by ELISPOT analysis. Cells were plated at 10⁵ cells/well and run in duplicate. SFC, spot-forming cells. (D) Epitope specificities were mapped using a matrix of HIV peptide pools. Responses to pools of HIV Gag (top), Pol (middle), and Nef (bottom) peptide are displayed, with specific, deconvoluted responses labeled. (E) Multiplex analysis of CIRC0196 HST cells reveals levels of cytokine secretion in response to GNP pepmix. (F) A chromium-51 release cytotoxicity assay was used to assess the ability of HST cells to kill autologous PHA blasts (PHAb) pulsed with GNP pepmix at various effector-to-target ratios. The results shown are representative of two independent experiments.

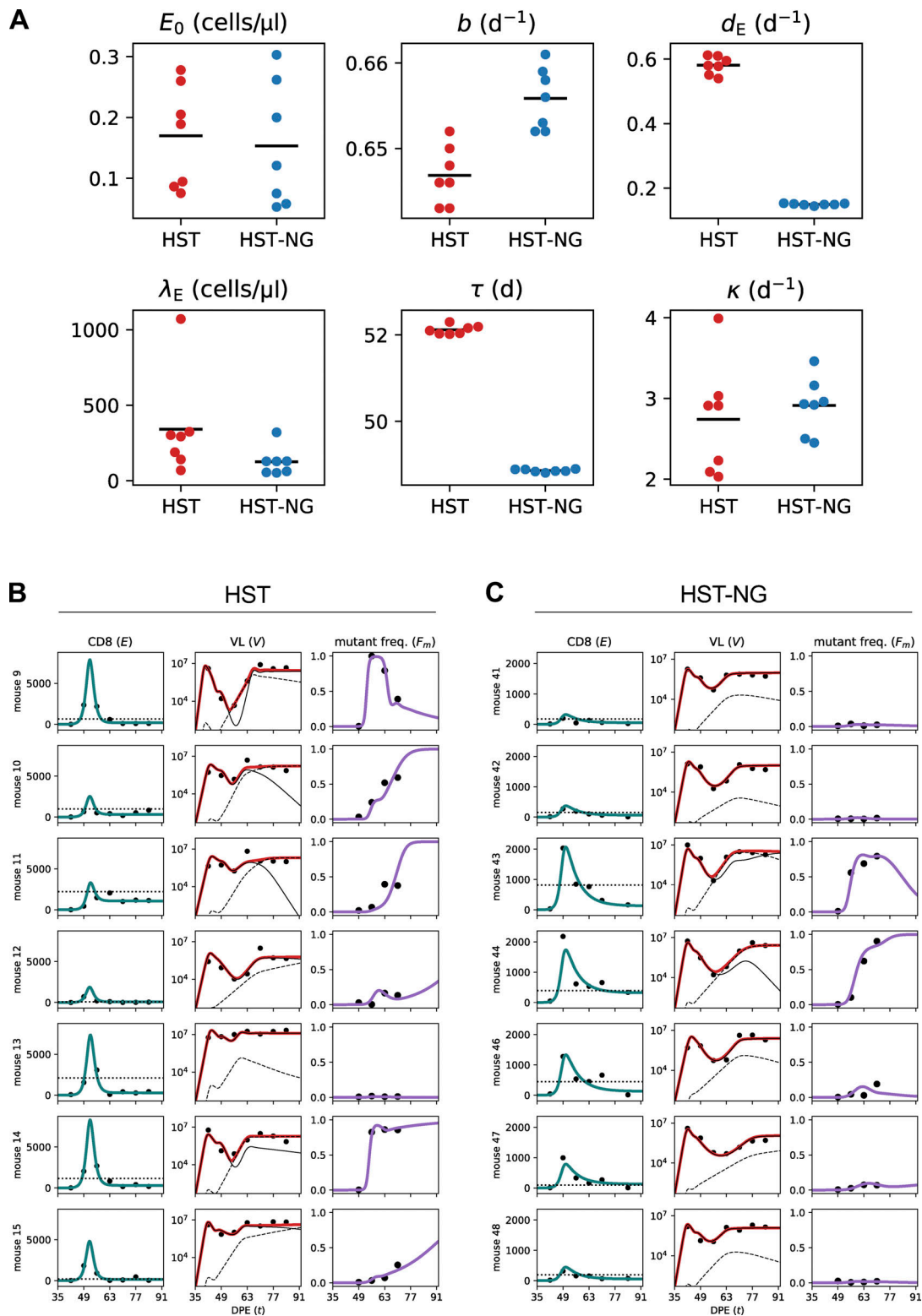


Figure S4. **Parameter estimates and model fits grouped by treatment for each individual mouse.** (A) Shown are the CD8⁺ T cell initial concentration (E_0), the expansion rate (b), the contraction rate (d_E), the steady-state concentration (λ_E), the time expansion stops (τ), and the maximal killing rate (κ). The horizontal bars indicate the population mean of the parameter estimates. As determined by model selection using AIC, the treatment group was added as a fixed effect to the parameters b , d_E , λ_E , and τ . (B and C) Fits of the ODE model for all mice treated with HST and HST-NG. Plots of individual mice from HST (A) or HST-NG (B) treatment groups. The left panels indicate the CD8⁺ T cell concentrations and the model prediction E (teal line). The horizontal dotted line indicates the CD8⁺ T cell concentration at which the killing rate is at half maximum. The middle panels show the plasma VL data and the predicted total VL (red line). The solid and dashed black curves indicate the contribution to the VL of the WT virus (V_w) and CD8⁺ T cell escape mutant virus (V_m), respectively. The right panels show the measured frequency of the CD8⁺ T cell escape mutant and its predicted frequency $F_m = V_m / (V_w + V_m)$. DPE, days post engraftment.

A

Table. Study participant demographics and clinical characteristics

Participant ID	Age	Sex	Ethnicity	ART regimen	Viral load (copies/ml)	Duration of viral load <50 copies/ml (months)
OM5220	54	Male	Asian	ABC, 3TC, DTG	<50	94
CIRC0196	56	Male	White	ABC, 3TC, DTG	<50	36

ABC, abacavir; 3TC, lamivudine; DTG, dolutegravir.

B

CIRC0196 - Medical Hx

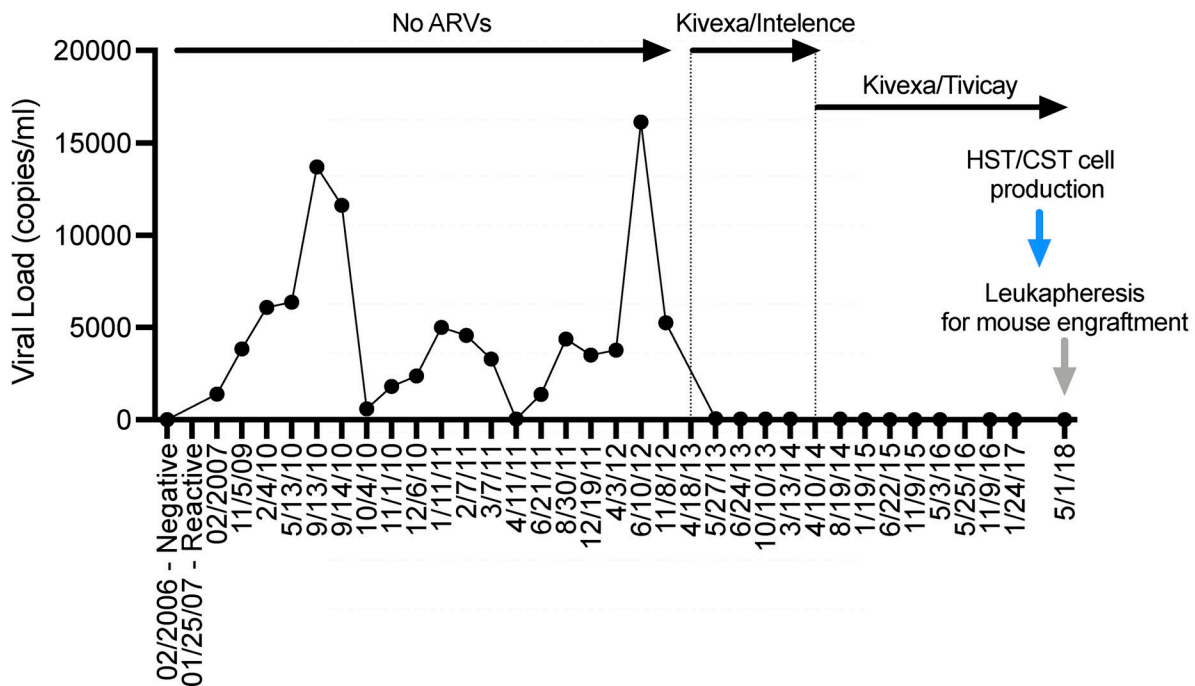


Figure S5. **Clinical data of study participants used in the generation of PDX mice. (A)** Summary demographics and clinical data. **(B)** Longitudinal VL data for study participant CIRC0196 showing partial control of viremia before ARV initiation. Hx, history; CST, CMV-specific T cell .